


## Depinning and flow of a vortex line in a uniaxial random medium

Federico Elías<sup>\*</sup> and Alejandro B. Kolton<sup>†</sup>

Centro Atómico Bariloche and Instituto Balseiro, CNEA,  
CONICET and Universidad Nacional de Cuyo, 8400 Bariloche, Argentina

Kay Jörg Wiese<sup>‡</sup>

Laboratoire de physique, Département de physique de IENS, Ecole normale supérieure,  
UPMC Univ. Paris 06, CNRS, PSL Research University, 75005 Paris, France

 (Received 19 April 2022; revised 17 June 2022; accepted 21 June 2022; published 30 June 2022)

We study numerically and analytically the dynamics of a single directed elastic string driven through a three-dimensional disordered medium. In the quasistatic limit the string is super-rough in the direction of the driving force, with roughness exponent  $\zeta_{\parallel} = 1.25 \pm 0.01$ , dynamic exponent  $z_{\parallel} = 1.43 \pm 0.01$ , correlation-length exponent  $\nu = 1.33 \pm 0.02$ , depinning exponent  $\beta = 0.24 \pm 0.01$ , and avalanche-size exponent  $\tau_{\parallel} = 1.09 \pm 0.03$ . In the transverse direction we find  $\zeta_{\perp} = 0.5 \pm 0.01$ ,  $z_{\perp} = 2.27 \pm 0.05$ , and  $\tau_{\perp} = 1.17 \pm 0.06$ . Our results show that transverse fluctuations do not alter the critical exponents in the driving direction, as predicted by the planar approximation (PA) proposed by Ertas and Kardar (EK) [*Phys. Rev. B* **53**, 3520 (1996)]. We check the PA for the measured force-force correlator, comparing to the functional renormalization-group and numerical simulations. Both random-bond (RB) and random-field (RF) disorder yield a single universality class, indistinguishable from the one of an elastic string in a two-dimensional random medium. While relations  $z_{\perp} = z_{\parallel} + 1/\nu$  and  $\nu = 1/(2 - \zeta_{\parallel})$  of EK are satisfied, the transversal movement is that of a Brownian, with a clock set locally by the forward movement. This implies  $\zeta_{\perp} = (2 - d)/2$ , distinct from EK. Finally, at small driving velocities the distribution of local parallel displacements has a negative skewness, while in the transverse direction it is a Gaussian. For large scales, the system can be described by anisotropic effective temperatures defined from generalized fluctuation-dissipation relations. In the fast-flow regime the local displacement distributions become Gaussian in both directions and the effective temperatures vanish as  $T_{\text{eff}}^{\perp} \sim 1/\nu$  and  $T_{\text{eff}}^{\parallel} \sim 1/\nu^3$  for RB disorder and as  $T_{\text{eff}}^{\perp} \approx T_{\text{eff}}^{\parallel} \sim 1/\nu$  for RF disorder.

DOI: [10.1103/PhysRevB.105.224209](https://doi.org/10.1103/PhysRevB.105.224209)

### I. INTRODUCTION

Many driven systems display a depinning transition from a static to a sliding state, at a finite value of an applied force or stress. Examples are field-driven domain walls in ferromagnetic [1–3] or ferroelectric materials [4,5], cracks under stress in heterogeneous materials [6–8], contact lines of liquids on a rough substrate [9,10], imbibition of fluids in porous and fractured media [11], reaction fronts in porous media [12], solid-solid friction [13], sheared amorphous solids or yield-stress fluids [14], dislocation arrays in sheared crystals [15], current-driven vortex lattices in superconductors [16–22], skyrmion lattices in ferromagnets [23], or earthquake models [24,25]. Among these systems, the family of *directed elastic manifolds in random media*, where interactions between constituents are purely elastic, and topological defects absent, have become the framework of choice for understanding quantitatively universal properties of the depinning transition [16,26–28].

Directed elastic manifolds embedded in a space of dimension  $D$  have an internal dimension  $d$  and an  $N$ -dimensional displacement field, such that  $D = N + d$ .<sup>1</sup> We focus on the overdamped zero-temperature dynamics when the manifold is driven by a force  $f$  in one of the  $N$  directions in a quenched random potential. In such a case, the competition of elasticity and disorder yields a critical force  $f_c$ , such that for  $f < f_c$  the steady-state velocity vanishes,  $v = 0$ , while for  $f > f_c$  the interfaces slide according to a velocity-field characteristics  $v(f) > 0$ . While one can impose the force  $f$  and then measure the velocity  $v(f)$ , in most experiments the driving velocity  $v$  is imposed, and the pinning force  $f$  measured. This is achieved by confining the elastic manifold within a quadratic potential, given by the demagnetization field in magnets, gravity in contact-line depinning, or the bulk elasticity in earthquakes.

The case  $(d, N) = (d, 1)$  of a directed elastic interface has been studied in detail [29–32]. It was found that the depinning transition at  $f_c$  is continuous, reversible, and occurs at a well-defined characteristic threshold force  $f_c$  [33], below which the interface remains pinned in a metastable state. At  $f_c$  the interface is marginally blocked and the instability is

<sup>\*</sup>federico.elias@cab.cnea.gov.ar

<sup>†</sup>alejandro.kolton@cab.cnea.gov.ar

<sup>‡</sup>wiese@lpt.ens.fr

<sup>1</sup>See [16] for a general description.

described by a localized soft spot or eigenvector [34]. Just above the threshold, the mean velocity  $v$  is given by the depinning law  $v \sim (f - f_c)^\beta$ , with  $\beta$  a nontrivial critical exponent. A divergent correlation length  $\xi \sim (f - f_c)^{-\nu}$  and a divergent correlation time  $\tau \sim \xi^z$  characterize the jerky motion as we approach  $f_c$  from above. Below the length scale  $\xi$  the interface is self-affine, with the displacement field growing as  $u \sim x^\zeta$ . Similarly,  $v \sim \xi^{\zeta-z}$  and  $\beta = \nu(z - \zeta)$ . The critical exponents have been estimated analytically [35–37] and numerically [31,38–42]. The different universality classes are distinguished by  $d$ , the range [43–47] or nature [48] of the elastic interactions, the anisotropic [49] or isotropic correlations of the pinning force [50,51], and by the presence of nonlinear terms in addition to the pinning force [49,52–56]. Boundary [57] or AC-driven [58] elastic interfaces have been studied as well. If the so-called statistical tilt symmetry (STS) holds, each depinning universality class has exactly two independent exponents  $\zeta$  and  $z$ . At large velocities, the disorder mimics thermal fluctuations with a velocity-dependent effective temperature, vanishing in the infinite-velocity limit. The particular case  $(d, N) = (1, 1)$ , which represents an elastic line in a random medium, is relevant for bulk magnets [3,59], and magnetic domain walls in ultrathin ferrimagnetic materials at very low temperatures [60]. Variants are systems with long-ranged elasticity, as contact lines of liquid menisci [9,10] or planar crack propagation [8]. When STS is broken, an additional Kardar-Parisi-Zhang (KPZ) term is generated, as in reaction fronts in porous media [12].

The depinning transition of a one-dimensional directed elastic line with a two-dimensional scalar displacement field  $(d, N) = (1, 2)$  in a  $(D = d + N = 3)$ -dimensional medium is realized for an isolated flux line (FL) in a superconductor. The two-dimensional displacement field has one component  $u_{\parallel}$  parallel to the driving direction, and a perpendicular component  $u_{\perp}$ , while the string is directed in the  $x$  direction as shown in Fig. 1. For an overdamped dynamics the study of such a system has been pioneered by Ertas and Kardar more than 25 years ago [61]. Compared with the  $(d, N) = (1, 1)$  case of interface depinning considerable less progress has been made since then, with the exception of a precise study of the critical force in the case of isotropic disorder [62], relevant for superconductor applications [19,63]. This is due to the difficulties the flux-line problem presents in addition to an elastic interface (and fewer applications). Indeed, even for harmonic elasticity and uncorrelated disorder one has to deal with a two-component (vector) displacement field instead of the scalar displacement field of the interface. One of the important consequences of this difference is that Middleton’s theorems [64], which lie at the heart of functional renormalization-group (FRG) calculations for depinning [35,36,65,66], and which greatly accelerate numerical simulations [53,67], are not valid for the FL, making a precise study of its large-scale properties difficult. In addition, renormalization-group calculations rely on an expansion in  $\epsilon = 4 - d$ , with  $d = 1$  far away from the upper critical dimension. In Ref. [61] Ertas and Kardar postulated anisotropic scaling forms for the directions parallel and perpendicular to the driving, with exponents  $\zeta_{\perp}$ ,  $\zeta_{\parallel}$ ,  $z_{\perp}$ ,  $z_{\parallel}$ ,  $\nu$ ,  $\beta$ . The latter were calculated, both via FRG and via direct numerical simulations. They describe the anisotropic

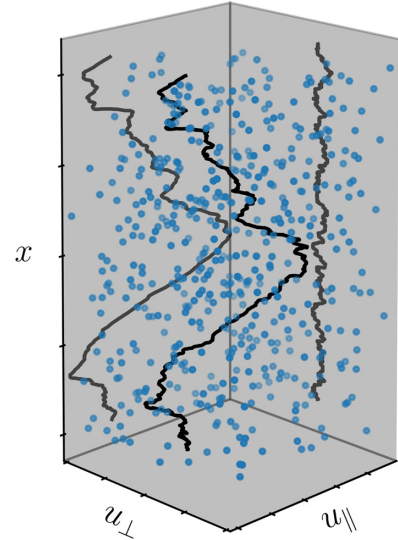


FIG. 1. Snapshot of an elastic line moving in an isotropic three-dimensional random environment. The projected profiles display the  $x$ -dependent displacements  $u_{\parallel}$  (parallel) and  $u_{\perp}$  (perpendicular) to the driving.

self-affine steady state of the line below the depinning correlation length  $\xi \sim (f - f_c)^{-\nu}$ ,

$$\langle [u_{\parallel}(x, t) - u_{\parallel}(0, 0)]^2 \rangle = x^{2\zeta_{\parallel}} g_{\parallel}(t/x^{z_{\parallel}}), \quad (1)$$

$$\langle [u_{\perp}(x, t) - u_{\perp}(0, 0)]^2 \rangle = x^{2\zeta_{\perp}} g_{\perp}(t/x^{z_{\perp}}), \quad (2)$$

with  $\beta = \nu(z_{\parallel} - \zeta_{\parallel})$  and  $g_{\parallel}(y)$  and  $g_{\perp}(y)$  universal functions.

The central idea of Ref. [61] by Ertas and Kardar (EK) is to propose a “planar approximation,” postulating that the exponents corresponding to the direction parallel to the driving are equal to those for  $N = 1$ , i.e., without a perpendicular direction. In a second step, exponents in the perpendicular direction are obtained, using the results in the parallel direction. EK then obtained the exponents  $\zeta_{\parallel} = 1$ , and  $\zeta_{\perp} = \zeta_{\parallel} - d/2 = \frac{1}{2}$ , using a FRG calculation at one-loop order (followed by a numerical check).

They then claimed that this result holds to all orders in perturbation theory, using an argument advanced in 1993 for  $N = 1$  by Narayan and Fisher [30], and in agreement with numerical simulations at the time. In the meantime it has been established that for  $N = 1$  the exponent  $\zeta > 1$ : The two-loop FRG [35,36] calculation of 2000 points out a mechanism absent from [30], which invalidates the argument for  $\zeta \equiv (4 - d)/3$  at depinning, while the latter remains valid in equilibrium. On the numerical side, it was shown that  $\zeta > 1$  [53,68]. The two-point function for the single displacement component  $u$  then becomes dependent on the system size  $L$  in the  $x$  direction, behaving as ( $\mathcal{A}$  is a number)

$$\langle [u(x, t) - u(0, t)]^2 \rangle = \mathcal{A}|x|^{2\zeta} L^{2\zeta-2}, \quad (3)$$

which can easily be misinterpreted as  $\zeta = 1$ . The most precise current value is  $\zeta = 1.25$  [42,69], and probably exactly  $\zeta = \frac{5}{4}$  [28,70]. Assuming Ertas and Kardar to keep  $\zeta_{\parallel}|_{N>1} = \zeta|_{N=1}$ , one may wonder whether they would keep the relation of  $\zeta_{\perp} = \zeta_{\parallel} - d/2$ , or replace it as well.

In this paper we revisit the problem of depinning and flow of an elastic string in three dimensions using numerical simulations and analytical arguments to address the above issues. Both for RB and RF disorder we confirm the validity of the anisotropic scaling forms and of the planar approximation for an extended set of exponents, together with the scaling relation  $z_{\perp} = z_{\parallel} + 1/\nu$  between dynamic exponents, as predicted in Ref. [61]. Our results agree with the “improved” EK relation  $\zeta_{\parallel} = \zeta|_{N=1} = 1.25$ , while our perpendicular roughness is  $\zeta_{\perp} = 0.5 \pm 0.001$ . We shall argue below that this is simply the thermal exponent of a  $d$ -dimensional elastic system,

$$\zeta_{\perp} = \frac{2-d}{2}. \quad (4)$$

We also calculate the force-force correlator, the avalanche-size, and waiting-time distributions, as well as the joint distribution of the two components of the center-of-mass jumps in the quasistatic regime. We finally unveil a skewed distribution of local parallel displacements at low velocities, and show that the dynamical structure of the string at large scales has nontrivial features.

The large-velocity or fast-flow regime of elastic manifolds, usually considered trivial, present nevertheless interesting open issues. Using a perturbative analysis, Koshelev and Vinokur [71] introduced the concept of shaking temperatures for moving vortex lattices by considering the effect of disorder as an effective thermal noise in the comoving frame. Later on, for the same problem, it was numerically shown that an effective velocity-dependent temperature can be defined from generalized fluctuation-dissipation theorems [72]. A similar analysis can be performed for the fast-flow regime of elastic manifolds in general. For interfaces with harmonic elasticity in isotropic media, functional renormalization-group (FRG) calculations show that the large-scale structure is well described by the Edwards-Wilkinson equation with an effective temperature  $T$  which, at large velocities, vanishes as  $T \sim 1/\nu$  [32]. In contrast, a perturbative analysis for a single vortex line finds that the shaking temperature is zero in the longitudinal direction and vanishes as  $1/\nu$  in the transverse direction [16], contradicting the FRG prediction [32] for interfaces in combination with the planar approximation. Moreover, a single monomer driven in a two-dimensional disordered medium which may be thought of as the limiting case of very short correlation lengths along  $x$ , shows an effective temperature vanishing as  $1/\nu^3$  in the parallel direction and  $1/\nu$  in the transverse direction [73], hence adding a third different prediction for the same property. Understanding these apparent discrepancies is an open issue we address here.

We find that in the comoving frame the system can accurately be described by two effective temperatures, defined from a generalized fluctuation-dissipation relation. In particular, at large velocities  $\nu$ , for microscopic disorder of the random-bond (RB) type, this effective temperature vanishes as  $T_{\text{eff}}^{\perp} \sim 1/\nu$  in the transversal direction, and as  $T_{\text{eff}}^{\parallel} \sim 1/\nu^3$  in the driving direction, while for microscopic disorder of the random-field (RF) type we find  $T_{\text{eff}}^{\parallel} \sim T_{\text{eff}}^{\perp} \sim 1/\nu$ . Interestingly, applying the EK planar approximation in the fast-flow regime, the dependency on  $\nu$  of the effective temperatures in the RB case is incompatible with the longitudinal “shaking temperature” obtained from a perturbative analysis [16], and

the effective “Edwards-Wilkinson” temperature  $\sim 1/\nu$  predicted in Ref. [32]. Nevertheless, the latter prediction agrees with our result for microscopic RF disorder. Finally, for RB disorder we confirm that with increasing  $\nu$  the aspect ratio of the string width changes from being elongated in the driving direction, to being elongated in the perpendicular direction, as qualitatively predicted by Scheidl and Nattermann [16]. In contrast, the change of aspect ratio disappears for RF disorder which crosses over from anisotropic fluctuations at intermediate velocities to isotropic ones at large velocities.

This paper is organized as follows: In Sec. II A we describe the model, the protocol, and its numerical implementation. In Sec. II B we define the observables of interest. Section III summarizes the theoretical results confirmed in our simulations, and proposes a mechanism for the perpendicular direction. Due to its simplicity, we are able to predict many observables analytically. In Sec. IV the main results are presented, followed by conclusions in Sec. V.

## II. MODEL AND OBSERVABLES

### A. Model and implementations

We study a driven one-dimensional elastic line (string), directed along the  $x$  direction, in a three-dimensional space at zero temperature. It is parametrized by the time-dependent two-dimensional vector field  $\mathbf{u}(x, t) = \{u_{\parallel}(x, t), u_{\perp}(x, t)\}$  which measures its continuum displacements along the parallel and perpendicular directions with respect to the driving direction (Fig. 1). The overdamped dynamics of the system is

$$\eta \partial_t \mathbf{u}(x, t) = c \partial_x^2 \mathbf{u}(x, t) + \mathbf{F}(x, \mathbf{u}(x, t)) + \mathbf{f}(\mathbf{u}(\mathbf{x}, \mathbf{t})). \quad (5)$$

Here  $\eta$  and  $c$  are the friction and elastic constants,  $\mathbf{f}(\mathbf{u})$  is the driving force, and  $\mathbf{F}_p(\mathbf{u}, x)$  is a statistically isotropic random pinning force in the  $\{u_{\parallel}, u_{\perp}\}$  plane. Equation (5) is a minimal model for a single vortex line in a type-II superconductor induced by a magnetic field pointing in the  $x$  direction [74,75]. The left-hand side then represents Bardeen-Stephen friction. The first term on the right-hand side is a harmonic approximation for the elastic tension of a single vortex, the second the coupling to the defects in the material, and the third a force due to a uniform applied current or some other way to impose a uniform mean velocity. In this work, to impose a steady-state mean velocity along the  $u_{\parallel}$  direction  $\mathbf{v} = \{v, 0\}$  we use a moving parabolic trap

$$\mathbf{f}(\mathbf{u}) = m^2[\mathbf{w}(t) - \mathbf{u}] \quad (6)$$

with  $\mathbf{w}(t) = \{w, 0\} = \{vt, 0\}$  and  $m \sim 1/L$ , with  $L$  the size of the string. With this driving protocol, both the instantaneous center-of-mass velocity and the driving force fluctuate, as they do in most experiments. We checked that the fixed-force ensemble (i.e., the one obtained by using a fixed force  $\mathbf{f} = \{f, 0\}$ , and where the center-of-mass velocity fluctuates) yields equivalent results for large enough systems (see Appendix A). Moreover, driving with a confining potential allows us to measure the effective force correlator, the central object of functional renormalization-group calculations [28,59,76–79].

For RB disorder, we consider a pinning force  $\mathbf{F} = \{F_{\parallel}, F_{\perp}\} = \{-\partial_{u_{\parallel}} V, -\partial_{u_{\perp}} V\}$  derived from a pinning potential

with correlations

$$\overline{V(\mathbf{x}, \mathbf{u})V(\mathbf{x}', \mathbf{u}')} = \delta(x - x')R(\mathbf{u} - \mathbf{u}'), \quad (7)$$

where  $\overline{(\dots)}$  denotes average over disorder realizations and  $R(u)$  is assumed to be a short-ranged function.

For RF disorder we use

$$\overline{F_\alpha(\mathbf{x}, \mathbf{u})F_\beta(\mathbf{x}', \mathbf{u}')} = \delta_{\alpha\beta} \Delta(|\mathbf{u} - \mathbf{u}'|)\delta(x - x'), \quad (8)$$

and  $\Delta(u)$  a short-ranged correlated function. Note that this type of disorder is not conservative, thus may allow a monomer  $x$  to perform periodic orbits even in the presence of a finite viscosity. As an alternative, we could use Eq. (7), with  $R(u) \sim |u|$ . This could be done by generating Fourier modes for the disorder, multiplying it with an appropriate kernel, and then Fourier transforming. We will not do this since it is (i) prohibitively costly to implement, and (ii) not necessary close to the depinning transition. Indeed, we show below that as long as  $m$  is sufficiently small, if a monomer position  $\mathbf{u}(\mathbf{x})$  is updated,  $u_{\parallel}(x)$  necessarily increases, forbidding periodic orbits. Both potentials represent isotropic disorder in the  $\mathbf{u}$  plane (“model A” in Ref. [61]).

We discretize the system along the  $x$  direction, such that  $\partial_x^2 \mathbf{u} \rightarrow \mathbf{u}(x+1) + \mathbf{u}(x-1) - 2\mathbf{u}(x)$ , and implement different uncorrelated pinning potentials on the resulting layers  $x = 1, \dots, L$ , with periodic boundary conditions. We use dimensionless units with  $\eta = c = 1$  and  $R(0) = \Delta(0) = O(1)$ .

For computational convenience two different implementations for RB disorder were used, one for finite velocities, and the other for the quasistatic  $v \rightarrow 0^+$  limit:

(i) At finite velocities we directly solve Eq. (5) using standard finite-difference techniques, and consider for each monomer  $x$  the  $V(\mathbf{u})$  to be the sum of Gaussian wells randomly distributed according to a Poissonian distribution.

(ii) In the quasistatic limit the dynamics of the system becomes very slow, and the direct integration of Eq. (5) is computationally inefficient. We therefore use a cellular automaton. This algorithm is a generalization of the algorithm used in Ref. [80] for a particle dragged in a two-dimensional disordered landscape. Here we generate a random pinning-energy landscape in a cubic lattice, described by the integer indices  $\{x, n_{\parallel}, n_{\perp}\}$ , using a uniform  $[0, 1)$  box distribution on each site, with uncorrelated energies at different sites. The two-dimensional position of the monomers at each layer  $x$  is discretized on this grid, and thus given by two integers  $\mathbf{u}(x, t) = \{n_{\parallel}(x), n_{\perp}(x)\}$ . For a given configuration we compute the total energy of each monomer in all nine nearest-neighboring positions, keeping the monomers of neighboring layers fixed. This energy for layer  $x$  is the sum of the random pinning energy, the quadratic potential well with curvature  $m^2$  centered at  $\{w, 0\}$ , and the elastic energy involving layers  $x+1$  and  $x-1$ . In an iteration, each monomer moves to the neighboring site with the lowest energy. This elementary step is performed synchronously for all  $x$  and repeated  $M$  times for a fixed  $w$ . In the quasistatic limit,  $M$  is chosen  $\infty$ , i.e.,  $\mathbf{w}$  is increased only after the string gets stuck. For  $v > 0$ ,  $M > 1$  is fixed (i.e., we let the string make  $M$  steps for each step  $\delta w$  in  $w$ ). This protocol simulates a velocity that fluctuates around the mean velocity  $v \sim \delta w/M$ . We checked that this algorithm yields, in the low-velocity limit, the same universal results as the direct integration of the continuous displacements in the

smooth pinning potential. Although most of our results are for RB disorder, we give some results, both for low and high velocities, for a RF type of disorder in order to detect possible dependencies on the microscopic disorder.

## B. Observables of interest

We now define some observables of interest. The steady-state force-velocity characteristics  $f(v)$  is computed from the mean force in the steady state,

$$f(v) = m^2[v t - u_{\parallel}(t)]. \quad (9)$$

Here  $u_{\parallel}(t)$  is the parallel component of the center-of-mass position

$$\mathbf{u}(t) = \langle \mathbf{u}(x, t) \rangle \quad (10)$$

with  $\langle (\dots) \rangle := L^{-1} \int dx (\dots)$ . The velocity-force characteristics, and in particular the critical force  $f_c := \lim_{v \rightarrow 0} f(v)$ , have a well-defined scaling behavior when  $m \rightarrow 0$  [76]. For small  $v$ , we expect  $v \sim [f(v) - f_c]^\beta$ .

To characterize the geometry of the string we define the mean quadratic widths in both directions

$$W_\alpha^2(t) = \overline{[u_\alpha(x, t) - u_\alpha(t)]^2}, \quad (11)$$

with  $\alpha = \{\parallel, \perp\}$ . We also define the local displacement components with respect to the center of mass  $\delta u_\alpha(x, t) := u_\alpha(x, t) - u_\alpha(t)$  and consider their distributions

$$P_\alpha^u(s) = \overline{\delta[s - \delta u_\alpha(x, t)]}, \quad (12)$$

as well as the joint distribution

$$P^u(s_{\parallel}, s_{\perp}) = \overline{\delta[s_{\parallel} - \delta u_{\parallel}(x, t)]\delta[s_{\perp} - \delta u_{\perp}(z, t)]}. \quad (13)$$

We define the anisotropic structure factor as

$$\mathcal{S}_\alpha(q, t) = \overline{|u_\alpha(x, t)e^{-iqx}|^2}, \quad (14)$$

where  $\alpha = \{\parallel, \perp\}$  and  $q = 2\pi n/L$  with  $n = 0, \dots, L/2 + 1$ .

In the quasistatic  $v \rightarrow 0^+$  regime, we consider the center of mass

$$\mathbf{u}(t) \rightarrow \mathbf{u}(w) \quad (15)$$

as a function of  $w = vt$  instead of  $t$ . (Which object is referred to will be clear from the context.) For this we let the string relax completely before shifting  $w \rightarrow w + \delta w$ . To study avalanches, we compute the PDF

$$P_\alpha(S) = \overline{\delta[S - Lu_\alpha(w + \delta w) + Lu_\alpha(w)]}. \quad (16)$$

Discontinuous jumps of  $u_\alpha(w)$  versus  $w$  are identified as shocks or avalanches. They occur at a discrete set of points  $w = w_i$ , producing a finite set of jumps of sizes  $S_i^\alpha = L[u_\alpha(w_i + \delta w) - u_\alpha(w_i)]$ , each one measuring the effective number of sites involved in the avalanche. The “waiting time” between consecutive jumps is defined as  $\delta w_i = w_i - w_{i-1}$ . Although  $\delta w_i$  is not a time, it yields the true waiting times  $\delta w_i/v$  between successive avalanches in the  $v \rightarrow 0^+$  limit. We are interested in its distribution

$$P^w(s) = \frac{1}{N} \sum_{i=1}^N \delta(s - \delta w_i) \quad (17)$$

for a large sequence of  $N \gg 1$  avalanches.

Finally, we consider the steady-state force-force correlation function in the driving direction, defined as [41,76]

$$\Delta_{\alpha\beta}(w - w') = L^d [\overline{f_\alpha(w) f_\beta(w')} - \overline{f_\alpha(w)} \overline{f_\beta(w')}], \quad (18)$$

where  $f_{\parallel}(w) := m^2[w - u_{\parallel}(w)]$  is the (spatially averaged) parallel force for each metastable state at fixed  $w$ , and  $f_{\perp}(w) = -m^2 u_{\perp}(w)$  is the perpendicular force. Due to symmetry, the cross correlator  $\Delta_{\parallel\perp}(w)$  vanishes, and we are left with two (*a priori*) independent correlation functions. From the correlation theorem these functions can be computed using the Fourier transform as  $\Delta = \mathcal{F}^{-1}\{|\hat{f}|^2\}$ , with  $f \xrightarrow{\mathcal{F}} \hat{f}$ . This quantity is a central object of the theory and can be compared quantitatively with FRG calculations and experiments [28,41,59,76–80].

### III. ANALYTICAL RESULTS

#### A. Analytical results for the planar approximation

EK consider a range of models, of which we focus on the simplest one, their *model A*. Their analysis is done in the force-controlled ensemble, with a constant driving force  $\mathbf{f} \equiv (f_{\parallel}, f_{\perp})$ , instead of the velocity-controlled ensemble we use in our model of Eq. (5). Since the arguments for both ensembles are equivalent, they apply to both cases. Hence, for the readers's convenience in this section we adopt the EK description. Omitting some additional terms, and changing to our notations, the essence of EK's equations (2.10a) and (2.10b) is

$$\eta \partial_t u_{\parallel}(x, t) = c \nabla_x^2 u_{\parallel}(x, t) + f_{\parallel} + F_{\parallel}(x, \mathbf{u}(x, t)), \quad (19)$$

$$\eta \partial_t u_{\perp}(x, t) = c \nabla_x^2 u_{\perp}(x, t) + f_{\perp} + F_{\perp}(x, \mathbf{u}(x, t)), \quad (20)$$

where  $\mathbf{F} \equiv (F_{\parallel}, F_{\perp})$  is the pinning force in Eqs. (5) and (8), and where a perpendicular driving force  $f_{\perp}$  is included according to Eq. (6), though the driving force in EK is purely in the parallel direction. EK then say in Eq. (3.2) that Eq. (19) can be reduced to

$$\eta \partial_t u_{\parallel}(x, t) = c \nabla_x^2 u_{\parallel}(x, t) + f_{\parallel} + \hat{F}(x, u_{\parallel}(x, t)), \quad (21)$$

where  $\hat{F}$  is a *reduction* of the pinning force  $F_{\parallel}$  to a function of  $x$  and  $u_{\parallel}$  only. EK argue that as long as  $F_{\parallel}(x, \mathbf{u})$  is short-ranged correlated, so will be  $\hat{F}(x, u_{\parallel})$ . We agree with their analysis, and would like to justify it as follows: If we assume the pinning energies to be bounded, so will be the possible forces. The critical force  $f_c$  becomes large for  $m \rightarrow 0$ , thus (in the cellular automaton model) each monomer can choose among the three forward neighbors, while the three backward neighbors as well as the two sideway neighbors can be neglected. The locally chosen force (including the elastic forces) is the maximum force among the three possible choices, i.e., the maximally possible descent in energy. That this image is correct, and each monomer only moves forward, is shown in Fig. 2, where we show that for small enough  $m^2$  a driven monomer at the center position ( $n = 4$  in the figure) has a finite probability  $P(n) = \frac{1}{3}$  to jump in any of the three forward directions ( $n = 2, 5, 8$  in the figure). In particular it never jumps backwards, or sideways.

As the minimum of three (correlated) random variables, we expect it to have (roughly) the same statistics as one of them

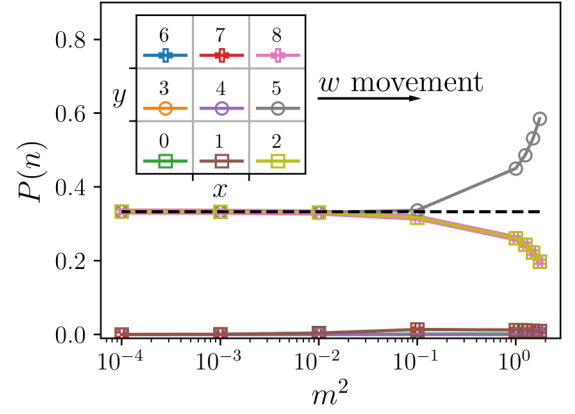


FIG. 2. In the cellular automaton model for the quasistatic regime, a monomer at position 4 (center of the inset) and driven in the  $x$  direction (to the right) by increasing the trap position  $w$ , can jump to its eight neighboring sites labeled by  $n \in \{0, 1, 2, 3, 5, 6, 7, 8\}$  (see inset). The main panel shows the jump probability  $P(n)$  as a function of the parabolic trap curvature  $m^2$ . For small  $m^2$  only  $n = 2, 5, 8$  have a finite and equal probability.

(say the middle one). Thus, it is short ranged, with a minimal history dependence. As an immediate consequence,

$$\zeta_{\parallel}|_{N \geq 2} = \zeta|_{N=1}. \quad (22)$$

For the line ( $d = 1$ ) this yields [28,69,70]

$$\zeta_{\parallel}|_{d=1} = \frac{5}{4}. \quad (23)$$

As for  $N = 1$ , the time-integrated response function is protected by the statistical tilt symmetry (STS) [30,61]

$$\zeta_{\parallel} + \frac{1}{v} = 2. \quad (24)$$

EK then argue that for the mean forces as a function of velocity,

$$\mathbf{f}(\mathbf{v}) = f(v)\hat{\mathbf{v}}, \quad \hat{\mathbf{v}} := \frac{\mathbf{v}}{v} \quad (25)$$

one has

$$\frac{\partial}{\partial v_{\parallel}} \mathbf{f}(\mathbf{v}) = \frac{\partial f(v)}{\partial v} \begin{pmatrix} 1 \\ 0 \end{pmatrix}, \quad (26)$$

$$\frac{\partial}{\partial v_{\perp}} \mathbf{f}(\mathbf{v}) = \frac{f(v)}{v} \begin{pmatrix} 0 \\ 1 \end{pmatrix}. \quad (27)$$

The only nonvanishing components are

$$\frac{\partial}{\partial v_{\parallel}} f_{\parallel}(\mathbf{v}) = \frac{df(v)}{dv}, \quad (28)$$

$$\frac{\partial}{\partial v_{\perp}} f_{\perp}(\mathbf{v}) = \frac{f(v)}{v}. \quad (29)$$

Using that  $v \sim (f_{\parallel} - f_c)^{\beta}$ ,  $\beta = v(z_{\parallel} - \zeta_{\parallel})$ , this leads to the scaling of timescales in the two directions

$$\tau_{\parallel} \sim \frac{\xi^2}{\frac{df(v)}{dv}} \sim \xi^{2+(\beta-1)/v} = \xi^{z_{\parallel}}, \quad (30)$$

$$\tau_{\perp} \sim \frac{\xi^2}{\frac{f(v)}{v}} \sim \xi^{2+\beta/v} = \xi^{z_{\perp}}. \quad (31)$$

As a consequence

$$z_{\perp} = z_{\parallel} + \frac{1}{\nu} \equiv z_{\parallel} + 2 - \zeta_{\parallel}. \quad (32)$$

While EK follow NF [30] in introducing a mean-field theory, and then expanding around it, this was not necessary in the field-theoretic work of Refs. [35,36,81]. Here we follow the latter approach. What is yet missing is a treatment of the transversal directions. We write this in differential form as

$$\eta du_{\perp}(x, t) = [c\nabla^2 u_{\perp}(x, t) - m^2 u_{\perp}(x, t)]dt + dF_{\perp}(x, u_{\parallel}). \quad (33)$$

The last term can be rewritten in different ways:

$$\begin{aligned} dF_{\perp}(x, u_{\parallel}) &= \partial_{u_{\parallel}} F_{\perp}(x, u_{\parallel}) du_{\parallel} \\ &= \partial_{u_{\parallel}} F_{\perp}(x, u_{\parallel}) \partial_t u_{\parallel}(x, t) dt. \end{aligned} \quad (34)$$

We now suppose that  $\partial_{u_{\parallel}} F_{\perp}(x, u_{\parallel})$  is a white noise in  $u_{\parallel}$ , so that

$$dF_{\perp}(x, u_{\parallel}) = \sqrt{\sigma} \kappa(x, u_{\parallel}) du_{\parallel}, \quad (35)$$

$$\langle \kappa(x, u) \kappa(x', u') \rangle = \delta^d(x - x') \delta(u - u'). \quad (36)$$

Alternatively, we can use a white noise in time,

$$dF_{\perp}(x, u_{\parallel}) = \sqrt{\sigma} \dot{u}_{\parallel}(x, t) \zeta(x, t) dt, \quad (37)$$

$$\langle \zeta(x, t) \zeta(x', t') \rangle = \delta^d(x - x') \delta(t - t'). \quad (38)$$

Let us derive some consequences of these equations. First of all, consider the motion of the center of mass of  $u_{\perp}(x, t)$ . We claim it satisfies the stochastic differential equation

$$\begin{aligned} \partial_t u_{\perp}(t) &:= \partial_t \frac{1}{L^d} \int_x u_{\perp}(x, t) \\ &= -m^2 u_{\perp}(t) + L^{-d/2} \sqrt{\sigma} \dot{u}_{\parallel}(t) \zeta(t), \end{aligned} \quad (39)$$

$$\langle \zeta(t) \zeta(t') \rangle = \delta(t - t'). \quad (40)$$

To prove the equivalence to Eqs. (37) and (38), one first checks the second moment of the driving term

$$\begin{aligned} &\left\langle \frac{1}{L^d} \int_x \sqrt{\sigma} \dot{u}_{\parallel}(x, t) \zeta(x, t) \frac{1}{L^d} \int_{y'} \sqrt{\sigma} \dot{u}_{\parallel}(y, t') \zeta(y, t') \right\rangle \\ &= \frac{1}{L^{2d}} \int_x \sigma \dot{u}_{\parallel}(x, t) \delta(t - t') \equiv \frac{\sigma}{L^d} \dot{u}_{\parallel}(t) \delta(t - t'). \end{aligned} \quad (41)$$

Second, one uses that the process is Gaussian, implying that this is the only relevant cumulant. In the same way, one derives that  $u_{\perp}(t)$  is a Gaussian process with variance (in the limit of  $m \rightarrow 0$ ),

$$\frac{1}{2} \langle [u_{\perp}(t) - u_{\perp}(t')]^2 \rangle = \frac{\sigma}{L^d} |u_{\parallel}(t) - u_{\parallel}(t')|. \quad (42)$$

At  $m > 0$ , the center of mass performs an Ornstein-Uhlenbeck process as a function of  $w$ . As a result we obtain (see Appendix B)

$$\begin{aligned} \Delta_{\perp\perp}(w) &:= m^4 L^d \overline{u_{\perp}(w' + w) u_{\perp}(w')^c} \\ &= \sigma m^2 e^{-m^2 w}. \end{aligned} \quad (43)$$

Equation (42) immediately implies relations (79) and  $s_{\perp} \sim \sqrt{\sigma_{\parallel}}$  observed in Fig. 8. More precisely

$$\langle S_{\perp}^2 \rangle|_{S_{\parallel}} = 2\sigma S_{\parallel}. \quad (44)$$

Let us finally address the question of the roughness exponent  $\zeta_{\perp}$ . Differential equations (33) and (35) yield

$$\frac{1}{2} \langle [u_{\perp}(x, u_{\parallel}) - u_{\perp}(x', u_{\parallel})]^2 \rangle = \sigma |x - x'|^{2\zeta_{\perp}}, \quad (45)$$

$$\zeta_{\perp} = \frac{2-d}{2}. \quad (46)$$

The parallel coordinate  $u_{\parallel}$  acts as a local time. The tricky point is whether this local time can be used as a global time. Our simulations show that this is indeed the case in  $d = 1$ .<sup>2</sup> Even if this cannot be rigorously asserted, we can show that the two-point function is indeed equivalent to the thermal one: The thermal equilibrium is characterized by a probability distribution of a monomer with coordinate  $u$ , given positions  $u_i, i = 1, \dots, n$ , of the  $n$  neighbors,

$$P(u|u_1, \dots, u_n) = \exp\left(-\frac{\sum_{i=1}^n (u - u_i)^2 + m^2 u^2}{2T_{\text{eff}}}\right). \quad (47)$$

It is achieved by a Langevin equation for a selected monomer with coordinate  $u$ , here written in a discretized form and a time step  $\delta t = 1$ :

$$u(t+1) - u(t) = \sum_{i=1}^n [u_i - u(t)] - m^2 u(t) + \sqrt{2T_{\text{eff}}} \eta_t, \quad (48)$$

$$\langle \eta_t \eta_{t'} \rangle = \delta_{t, t'}. \quad (49)$$

(This is a Kronecker  $\delta$ .) If the string (or manifold) is in thermal equilibrium, then running Eq. (48) for the selected monomer ensures that it remains in equilibrium. If it is not in equilibrium, then running Eq. (48) for the selected monomer ensures that it will get into equilibrium with its neighbors according to the measure (47). Running the same equation for each monomer in turn, and repeating the procedure for all monomers, one ensures that thermal equilibrium is reached for the whole string.

Let us finally comment on EK and their result that  $\zeta_{\perp} = \zeta_{\parallel} - d/2$ . There are several assumptions in their calculation which need to be questioned: The first and strongest is that  $\Delta(u_{\parallel}, u_{\perp})$  only depends on  $u_{\parallel}$ . The simplest interpretation is that  $\Delta(u_{\parallel}, u_{\perp})$  is constant in the perpendicular direction, or at least extremely long-ranged correlated, violating basic assumptions of the system, and the particle simulation in Ref. [80]. The next-to-simplest assumption is that  $\Delta(u_{\parallel}, u_{\perp}) = \Delta(u_{\parallel}) \delta(u_{\perp})$ , i.e., extremely short-ranged correlated. In this case, however, the transversal dependence needs to appear in the FRG equations, which it does not. In this context let us remind that when one starts with short-ranged correlated disorder for  $N = 1$  in a simulation, one can clearly

<sup>2</sup>We learned from Ponson [82] that the perpendicular roughness for fracture in  $d = 1$  is  $\zeta_{\perp} \simeq 0$ , consistent with the ‘‘thermal’’ exponent for LR elasticity  $\zeta_{\perp} = (1-d)/2$ .

see that  $\Delta(w)$  acquires a finite range as  $m$  is decreased. This is correctly described by the FRG.

Next, we are doubtful about the appearance of  $z_{\parallel}$  in EK's equation (6.16): We believe that since  $\Delta(u_{\parallel}, u_{\perp})$  is a static quantity, its renormalization cannot contain information about the dynamical exponents. Rather, the rescaling term in Eq. (6.16) should reduce to  $(\epsilon - 2\zeta_{\perp})C_{\perp}(u)$ , similar to what happens in Eq. (6.15), where the rescaling term simplifies to  $(\epsilon - 2\zeta_{\perp})C_{\perp}(u)$ . With this in mind, we can rewrite Eq. (6.16) as

$$\begin{aligned}\zeta_{\perp} &= \frac{4-d}{2} + z_{\parallel} - z_{\perp} \\ &= \begin{cases} \frac{4-d}{2} & \text{if } z_{\perp} \rightarrow z_{\parallel}, \\ \zeta_{\parallel} - \frac{d}{2} & \text{if } z_{\perp} \rightarrow z_{\parallel} + \frac{1}{\nu}. \end{cases}\end{aligned}\quad (50)$$

The first is the Larkin (dimensional-reduction) result, expected if the disorder is constant in space. The second is the one given by EK, which contradicts our result (46), and our numerical simulations [see Eq. (59)], while Eqs. (46) and (59) agree.

### B. Analytical results in the fast-flow regime

The standard argument for the amplitude of the two-point function in the fast-flow regime is constructed as follows: First, one considers the two-point function at equal times set to 0:

$$\langle u(q, 0)u(-q, 0) \rangle = \int_{t>0} \int_{t'>0} \Delta(v(t-t'))e^{-(q^2+m^2)(t+t')}. \quad (51)$$

For RF disorder, since  $\Delta(w)$  monotonically and faster than exponentially decays to 0 for increasing  $w$ , one can approximate for large  $v$

$$\Delta(vt) \simeq 2\mathcal{A}\delta(vt) \equiv \frac{2\mathcal{A}}{v}\delta(t), \quad (52)$$

$$\mathcal{A} := \int_0^{\infty} \Delta(w)dw. \quad (53)$$

With this, Eq. (51) reduces to

$$\begin{aligned}\langle u(q, 0)u(-q, 0) \rangle &\simeq \frac{2\mathcal{A}}{v} \int_{t>0} e^{-2(q^2+m^2)t} \\ &= \frac{T_{\text{eff}}^{\text{RF}}}{q^2+m^2}, \quad T_{\text{eff}}^{\text{RF}} = \frac{\mathcal{A}}{v}.\end{aligned}\quad (54)$$

For RB disorder, the situation is different as  $\Delta(w) = -R''(w)$ , where now  $R(w)$  is fast decaying. As a result

$$\begin{aligned}\Delta(v(t-t')) &= -R''(v(t-t')) \\ &= \frac{1}{v^2} \partial_t \partial_{t'} R(v(t-t')) \\ &\simeq -\frac{2\mathcal{B}}{v^3} \delta''(t),\end{aligned}\quad (55)$$

$$\mathcal{B} = \int_0^{\infty} R(w)dw. \quad (56)$$

A numerical simulation shows that thermal noise correlated as  $\delta''(t)$  leads to a nonvanishing variance for each site, uncorrelated between neighboring sites. It does not contribute to the

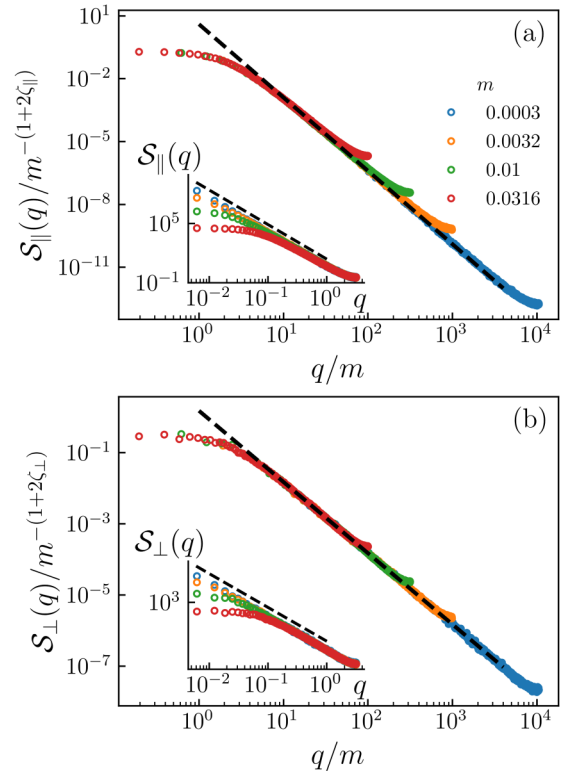


FIG. 3. Scaled structure factors for quasistatic motion as a function of confinement strength  $m$  for the parallel (a) and transverse (b) directions. Both directions display a self-affine structure up to the confinement length  $L_m \sim m^{-1}$ . Dashed lines in (a) and (b) correspond to power laws  $\mathcal{S}_{\parallel}(q) \sim q^{-(1+2\zeta_{\parallel})}$  and  $\mathcal{S}_{\perp}(q) \sim q^{-(1+2\zeta_{\perp})}$ , yielding the depinning roughness  $\zeta_{\parallel} \approx 1.25$  and  $\zeta_{\perp} \approx 0.5$ , respectively. Insets show raw data for each case.

structure factor. Thus, the leading contribution should come from Eqs. (52) and (53), where the renormalization-group (RG) flow from RB to RF is cut such that below, in Sec. IV F, we observe  $\mathcal{A} \simeq 1/v^2$ . A proper theoretical explanation remains outstanding.

For a single overdamped particle in a one-dimensional force field with a finite correlation length, we solve the problem analytically in Appendix C, yielding in agreement with the above scalings  $T_{\text{eff}}^{\text{RB}} \sim 1/v^3$  and  $T_{\text{eff}}^{\text{RF}} \sim 1/v$  at large velocities.

## IV. NUMERICAL RESULTS

### A. Steady state in the quasistatic regime

We start analyzing the geometry of the elastic string in the quasistatic steady-state regime, using the cellular automaton. In Fig. 3 we show the structure factors for the parallel (a) and perpendicular (b) directions, as a function of the parameter  $m$  in Eq. (6). Since  $v \rightarrow 0^+$ , the depinning correlation length  $\xi$  is not set by the distance to  $f_c$ , but by the confining potential  $\xi_m \approx \frac{1}{m}$ . Indeed, in both cases we observe that the string becomes flat beyond  $\xi$ , while below (but above the lattice constant here set to 1) a self-affine random-manifold regime is observed. The inset of the two figures validates the scalings

$$\mathcal{S}_{\alpha}(q) \sim q^{-(1+2\zeta_{\alpha})} G_{\alpha}(q\xi_m), \quad (57)$$

with  $G_\alpha(y) = \text{const}$  for  $y \ll 1$  ( $\xi_m \gg 1/q$ ) and  $G_\alpha(y) = y^{1+2\zeta_\alpha}$  for  $y \gg 1$  ( $\xi_m \ll 1/q$ ). These results also imply that  $W_\alpha^2 \sim \xi_m^{2\zeta_\alpha} \approx L^{2\zeta_\alpha}$  if  $mL$  is kept constant when increasing  $L$ . The roughness exponents in the two directions (see dashed lines) are different:

$$\zeta_{\parallel} = 1.25 \pm 0.01, \quad (58)$$

$$\zeta_{\perp} = 0.50 \pm 0.01. \quad (59)$$

These results are compatible with the earlier result of Ref. [71]. We find a value of  $\zeta_{\parallel} \approx \frac{5}{4}$ , indistinguishable from the roughness exponent of the driven one-dimensional quenched Edwards-Wilkinson interface obtained from numerical simulations [42,69], and consistent with two-loop functional renormalization-group calculations [35,36]. In the perpendicular direction the exponent is the same as for a moving line in presence of thermal noise. Both results are in agreement with our theoretical predictions in Eqs. (23) and (46).

The statistical tilt symmetry applied to the parallel direction implies that

$$\nu = \frac{1}{2 - \zeta_{\parallel}} = 1.33 \pm 0.02. \quad (60)$$

These results are consistent with the planar approximation of Ertas and Kardar [61], and with their one-loop analysis. As we discussed in Sec. III A, they are inconsistent with the higher-order results. In particular, they contradict EK's  $\zeta_{\perp} = 5\zeta_{\parallel}/2 - 2$  [61].

As the model of [61] and its numerical implementation are equivalent to ours, the numerical discrepancy can be explained by noting that the  $x$  and  $L$  dependence of the correlation function

$$B_\alpha(x, L) := \overline{[u_\alpha(x, t) - u_\alpha(0, t)]^2} |_L \quad (61)$$

used in Ref. [61] cannot detect roughness exponents larger than one for a fixed sample size  $L$ . As first observed in Ref. [68] for  $N = 1$  ( $\mathcal{A}$  is a number)

$$B(x, L) \simeq \mathcal{A}L^{2\zeta - 2}x^2 \quad \text{if } \zeta > 1, \quad (62)$$

$$B(x, L) \simeq \mathcal{A}x^{2\zeta} \quad \text{if } \zeta < 1. \quad (63)$$

Taking into account that  $\zeta_{\parallel} > 1$  and  $\zeta_{\perp} < 1$ , the first line applies to  $\zeta_{\parallel}$ , and the second to  $\zeta_{\perp}$ . Therefore, if we use the scaling  $B(x) \sim x^{2\zeta}$  to determine  $\zeta$ , its value is only correct when  $\zeta < 1$ , but saturates at 1 whenever  $\zeta > 1$ . (In practice, it is even difficult to see the exponent 1, and one tends to measure something slightly smaller [28].) We believe that this is what Ertas and Kardar [61] saw in their simulation.

Aside from validating the planar approximation, the results of Eq. (58) imply that whenever the harmonic elasticity is an approximation for a more complicated elasticity, the model becomes physically unrealistic for large enough sizes  $L$  because local slopes  $\overline{\langle (du_{\parallel}/dx)^2 \rangle} = B(1, L) \simeq L^{2\zeta_{\parallel} - 2}$  diverge with  $L$  [68]. This motivates one to either include anharmonic corrections to the elasticity, or other effects such as overhangs and pinch-off loops to the model. This notwithstanding, the predictions of Eq. (58) may describe the geometry at intermediate scales, below a putative crossover to a different regime.

This scenario is present in recent experiments on creep [83] and depinning [60] displaying super-rough magnetic domain walls in ultrathin ferromagnetic films.

### B. Relaxation from a flat initial condition in the quasistatic regime

In the quasistatic protocol we start with a flat initial condition  $\mathbf{u}(z, t) = \{u_0, 0\}$  such that  $m^2(w - u_0) = f_c$ . Since the flat string is uncorrelated from the disorder we also have  $v(t = 0) = f_c$ . As observed for interfaces relaxing at depinning [42], before reaching the steady state the string is in a universal transient regime, which yields information about the critical exponents of the steady-state depinning transition. In particular,  $u_{\perp}$  and  $u_{\parallel}$  each evolves with a different dynamical length  $\ell_{\parallel}(t) \sim t^{1/\zeta_{\parallel}}$  and  $\ell_{\perp}(t) \sim t^{1/\zeta_{\perp}}$ , controlling the relaxational dynamics.

Since the interface is initially flat,  $W_\alpha^2(t = 0) = 0$ . After a nonuniversal microscopic transient the global width reaches a universal transient regime described by  $W_\alpha^2(t) \sim \ell_\alpha(t)^{2\zeta_\alpha}$ , and hence

$$W_\alpha^2(t) \sim t^{2\zeta_\alpha/\alpha}. \quad (64)$$

This holds as long as  $\ell_\alpha(t) < \xi_m$ . On the other hand, at long times it saturates as  $W_\alpha^2(t) \sim \xi_m^{2\zeta_\alpha} \sim L^{2\zeta_\alpha}$  (the last relation holds provided  $mL$  is kept fixed). The power-law regime of Eq. (64) is confirmed in Fig. 4(a) where we show the evolution of  $W_{\parallel}^2(t)$  and  $W_{\perp}^2(t)$ . Using the known values of  $\zeta_{\parallel}$  [Eq. (58)] and  $\zeta_{\perp}$  [Eq. (59)] and by fitting in the appropriate (intermediate) range indicated in red, we get

$$z_{\parallel} = 1.43 \pm 0.01, \quad (65)$$

$$z_{\perp} = 2.27 \pm 0.05. \quad (66)$$

This validates the relation (32),

$$z_{\perp} = z_{\parallel} + 1/\nu, \quad (67)$$

predicted in Ref. [61], as  $z_{\parallel} + 1/\nu - z_{\perp} = -0.09 \pm 0.08$ . For reference, the analytical values proposed in [69] combined with the scaling relation (67) are

$$z_{\parallel} = \frac{10}{7} = 1.42857, \quad (68)$$

$$z_{\perp} = \frac{61}{28} = 2.17857. \quad (69)$$

In the same universal regime where Eq. (64) holds, the parallel center-of-mass velocity reaches a universal transient regime, where it vanishes as  $v(t) \sim \ell_{\parallel}(t)^{-\beta/\nu}$ , and hence

$$v(t) \sim t^{-\beta/\nu z_{\parallel}}. \quad (70)$$

In Fig. 4(b) we show the fit to this regime and obtain, knowing  $\nu$  from Eq. (60) and  $z_{\parallel}$  from Eq. (65),

$$\beta = 0.24 \pm 0.01. \quad (71)$$

This is indistinguishable from the result for the one-dimensional interface [42]. It is compatible with the exact relation [69]

$$\beta = \nu(z_{\parallel} - \zeta_{\parallel}) = \frac{5}{21} = 0.238095\dots \quad (72)$$



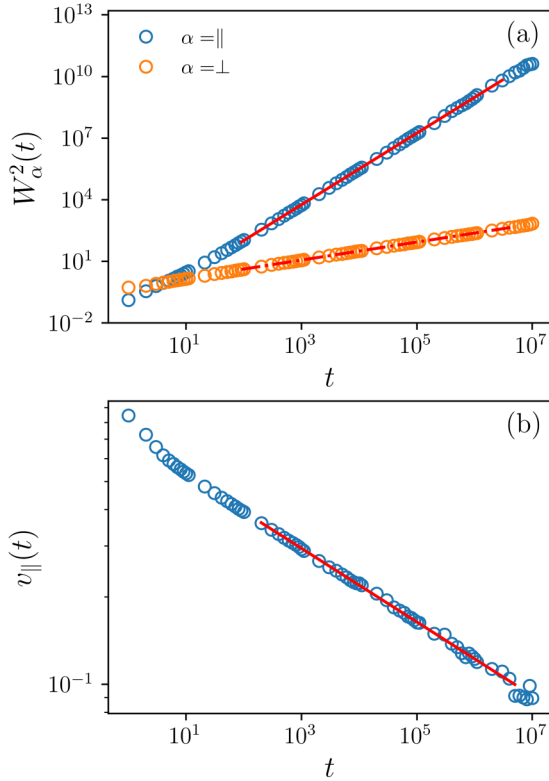


FIG. 4. Nonsteady relaxation of the roughness (a) and velocity (b) from a flat initial configuration at constant force  $f = f_c \approx 0.765$ , for a string with  $L = 2^{18}$  monomers, averaged over eight disorder realizations. Red lines show power-law fits in the universal relaxation regime. In (a) we fit  $W_\alpha^2(t) \sim t^{2\zeta_\alpha/z_\alpha}$  with  $\alpha = \parallel, \perp$  to obtain  $z_\parallel = 1.43 \pm 0.01$ ,  $z_\perp = 2.27 \pm 0.05$ . (b) From the relaxation of the mean velocity  $v \sim t^{-\beta/\nu z_\parallel} = t^{-(2-\zeta_\parallel)\beta/z_\parallel}$  we obtain  $\beta = 0.24 \pm 0.01$ .

To conclude, these results validate the exponent relations due to the planar approximation [61] in the modified form of Sec. III A.

Finally, a detailed geometrical view of the relaxation can be obtained from the structure factors. Using the exponents obtained in Fig. 5 we show that when  $\ell_\alpha(t) < \xi_m$  the evolution of the structure factors accurately follows the scaling

$$S_\alpha(q, t) \sim q^{-(1+2\zeta_\alpha)} F_\alpha(q\ell_\alpha(t)), \quad (73)$$

with  $F(x) = \text{const}$  for  $x \ll 1$ , and  $F(x) = x^{(1+2\zeta_\alpha)}$  for  $x \gg 1$ . Therefore, the string progressively becomes self-affine with exponents  $\zeta_\alpha$  up to the corresponding scales  $\ell_\alpha(t)$ . For larger distances, the memory of the flat initial condition is preserved.

### C. Depinning avalanches

We now describe the avalanche statistics in the quasistatic regime. We first compute the center-of-mass jumps, defined in Eq. (16). In the insets of Fig. 7 we see that jumps in both directions fairly follow a power-law decay with a cutoff

$$P_\alpha(S) \sim S^{-\tau_\alpha} G_\alpha(S/S_m^\alpha). \quad (74)$$

Here

$$S_m^\alpha := \frac{\langle S_\alpha^2 \rangle}{2\langle S_\alpha \rangle} \quad (75)$$

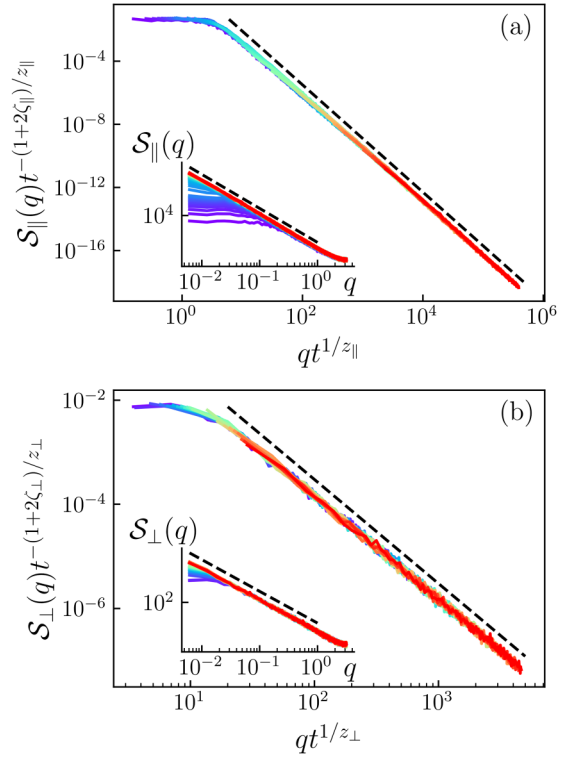


FIG. 5. Relaxation of the structure factors for  $L = 1024$  monomers and  $m^2 = 10^{-6}$ , showing  $S_\alpha(q) \sim q^{-(1+2\zeta_\alpha)} G_\alpha(qt^{1/z_\alpha})$  scaling, in both directions  $\alpha = \parallel, \perp$ . Dashed lines indicate power laws and insets show corresponding raw data. (a) Rescaled  $S_\parallel(q)$  from  $t = 10^3$  (violet) to  $t = 5 \times 10^7$  (red). The dashed line corresponds to  $z_\parallel = 1.43$  and  $\zeta_\parallel = 1.25$ . (b) Rescaled  $S_\perp(q)$  from  $t = 10^6$  (violet) to  $t = 5 \times 10^7$  (red). The dashed line corresponds to  $z_\perp = 2.18$  and  $\zeta_\perp = 0.5$ .

grows with decreasing  $m$ , and  $G_\alpha(x)$  are cutoff functions, such that  $G_\alpha(x) \sim \text{const}$  for  $x \ll 1$  and  $G_\alpha(x) \rightarrow 0$  roughly exponentially for  $x > 1$ . For the quantitative numerical analysis it is convenient [84] to define

$$s := \frac{S}{S_m}, \quad (76)$$

$$p_\alpha(s) := P_\alpha(S) \frac{S_m^2}{\langle S \rangle}. \quad (77)$$

From the main panel and the inset of Fig. 6 we see that the cutoffs respectively scale as

$$S_m^\parallel \sim m^{-(d+\zeta_\parallel)}, \quad d = 1 \quad (78)$$

$$S_m^\perp \sim \sqrt{S_m^\parallel}. \quad (79)$$

In Fig. 7 we show the master curves in the two directions, as obtained by rescaling those in the insets for different values of  $m$ . The collapse for different  $m$  is better in the parallel direction than in the perpendicular one, probably due to the smaller range of sizes for the latter. Nevertheless, we can fit the avalanche exponents for  $s < 1$  in both cases, leading to

$$\tau_\parallel = 1.09 \pm 0.03, \quad (80)$$

$$\tau_\perp = 1.17 \pm 0.06. \quad (81)$$

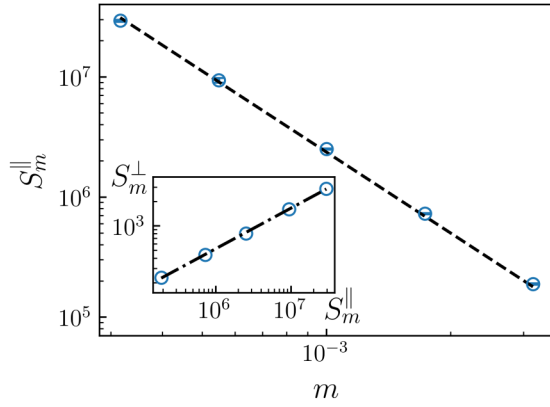


FIG. 6. Dependence of the avalanche-size cutoff  $S_m^\alpha$  with the confinement factor  $m$ . The dashed line corresponds to  $S_m^\parallel \propto m^{-(D+\zeta_\parallel)}$  with  $D = 1$ . Inset: the dotted-dashed line shows that cutoffs in each direction are strongly correlated as  $S_m^\perp \propto \sqrt{S_m^\parallel}$ .

The value of  $\tau_\parallel$  is consistent with the planar approximation, as numerical simulations of avalanches for one-dimensional interfaces present an indistinguishable value for  $\tau$  [84]. The scaling relation  $\tau = 2 - 2/(d + \zeta)$  of Narayan and Fisher [30] (for  $N = 1$ ) with the exponents of [69] [see Eq. (58)]

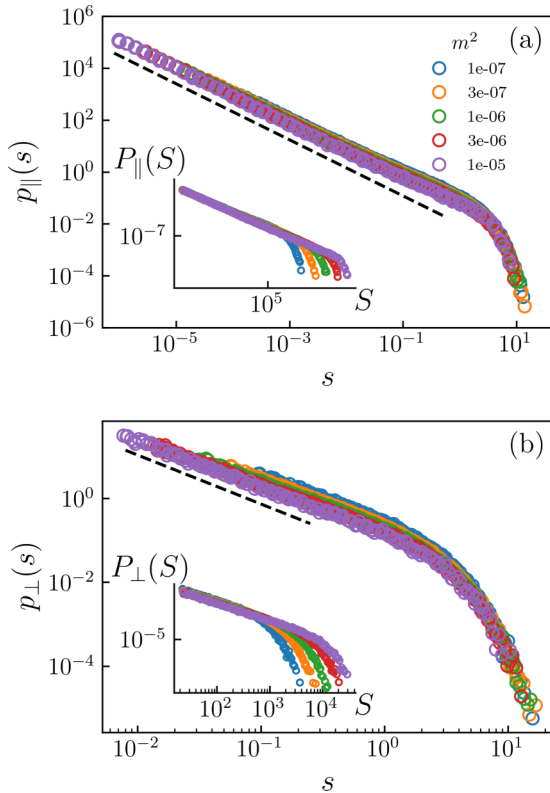


FIG. 7. Rescaled distribution of center-of-mass jumps for different  $m^2$  and  $L = 4096$  monomers in the parallel (a) and perpendicular (b) directions, according to Eq. (77). Dashed lines indicate power-law fits  $p_\alpha(s) \propto s^{-\tau}$  well below the cutoffs. Insets show raw data. The dashed line fits yield  $\tau_\parallel = 1.09 \pm 0.03$  (a) and  $\tau_\perp = 1.17 \pm 0.06$  (b).

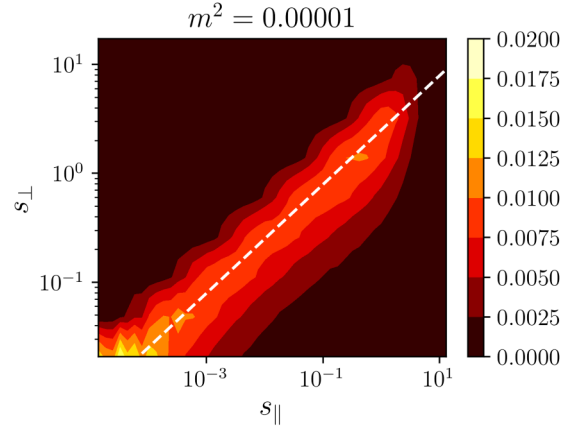


FIG. 8. Normalized count of events with center-of-mass jump sizes  $(s_\parallel, s_\perp)$ , highlighting their strong correlation. The white dashed line corresponds to  $s_\perp \propto \sqrt{s_\parallel}$ .

yields

$$\tau_\parallel = 2 - \frac{2}{d + \zeta_\parallel} \xrightarrow{d \rightarrow 1} \frac{10}{9} = 1.11111\dots \quad (82)$$

For the scalar model ( $N = 1$ ) this scaling relation was conjectured by Narayan and Fisher [30] assuming a finite density of avalanches at the depinning threshold. It was rederived in Ref. [66] from FRG. This result significantly differs from the mean-field result  $\tau_{\text{MF}} = \frac{3}{2}$ . Equation (82) was tested numerically [84] and analytically via one-loop FRG calculations [10].

To understand the value of  $\tau_\perp$ , we remind Eq. (44),  $\langle S_\perp^2 \rangle|_{s_\parallel} = 2\sigma s_\parallel$ . From this we immediately obtain the scaling relation (79) for  $S_m^\perp$ . We have analyzed the joint pair distribution function (PDF)  $p(s_\parallel, s_\perp)$  for a long sequence of avalanches (see Fig. 8). The strong correlation along the line  $s_\perp \sim \sqrt{s_\parallel}$  confirms Eq. (44). This allows us to write  $P_\parallel(S_\parallel)dS_\parallel = P_\perp(S_\perp)dS_\perp$  with  $S_\perp \sim S_\parallel^{1/2}$ . Assuming that for small arguments  $P_\parallel(S_\parallel) \sim S_\parallel^{-\tau_\parallel}$  and  $P_\perp(S_\perp) \sim S_\perp^{-\tau_\perp}$ , we obtain that

$$\tau_\perp = 2\tau_\parallel - 1 \xrightarrow{d \rightarrow 1} \frac{11}{9} = 1.22222\dots \quad (83)$$

The numerically obtained value reported in Eq. (81) is  $\tau_\perp = 1.17 \pm 0.06$ , in fair agreement with the one predicted by the scaling relation (83).

#### D. Waiting-time distribution

Consecutive avalanches are characterized by a “waiting-time” distribution  $P^w$  defined in Eq. (17). In Fig. 9 we show that this distribution follows an exponential decay, already observed in Ref. [85] ( $N = 1$ , equilibrium),

$$P^w(\delta w) \approx \frac{m^2}{\delta f^*} e^{-\delta w m^2 / f^*}, \quad (84)$$

with  $f^* \approx 0.000135$  a microscopic force. Therefore, our avalanches are characterized by a mean waiting distance  $f^*/m^2$ . If we choose  $L = \xi_m \approx 1/m$ , the mean waiting distance diverges with system size as  $\langle \delta w \rangle \sim L^2$ , implying a dominance of large-stress accumulation periods needed to

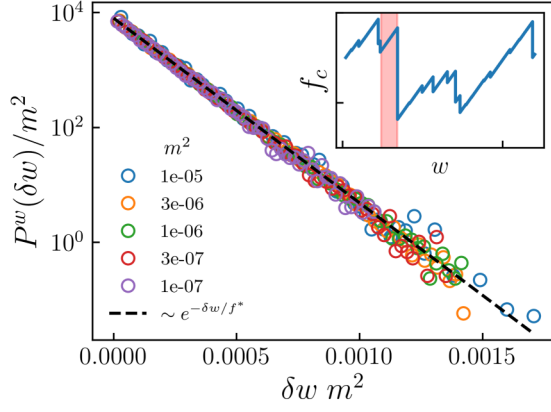


FIG. 9. Scaled “waiting-time” distribution between consecutive avalanches in the parallel direction. The dashed line indicates an exponential fit.

trigger large avalanches of size  $S_{\parallel} \sim L^{1+\zeta_{\parallel}}$ . Interestingly, a pure exponential distribution is also found for the “Gumbel” universality class of a driven particle in a short-range correlated random-force landscape [80]. This contrasts with the Weibull and Frechet universality classes. Nevertheless, the critical force distribution for one-dimensional interfaces in a box of size  $L \times L^{\zeta}$  is slightly different from Gumbel [86,87]. Since in our case we have (in the parallel direction) an aspect ratio  $\xi_m \times \xi_m^{\zeta}$  (with  $\xi_m \approx 1/m$ ) it would be interesting to derive  $P^w$  for such a distribution.

### E. Renormalized force-force correlator

Finally, we discuss the force-force correlator of Eq. (18), which is a central quantity in the renormalization-group calculations. In Fig. 10(a) we show that the correlator  $\Delta_{\parallel} \equiv \Delta_{\parallel,\parallel}$  for different  $m$  can be collapsed using  $\Delta_{\parallel}(w) \approx m^{\epsilon-2\zeta_{\parallel}} \tilde{\Delta}_{\parallel}(wm^{\zeta_{\parallel}})$  [76], with  $\epsilon = 4 - d = 3$  for our case and  $\zeta_{\parallel} = 1.25$  from Eq. (58).

By fitting  $\tilde{\Delta}_{\parallel}(x) = ce^{-ax-bx^2-dx^3}$  in the range  $w \in [0, 1]$  we obtain  $a = 2.38 \pm 0.07$ ,  $b = 0.8 \pm 0.2$ ,  $c = 0.188 \pm 0.001$ , and  $d = 0.09 \pm 0.21$ . As a consequence,  $\frac{\tilde{\Delta}_{\parallel}(0)\tilde{\Delta}_{\parallel}''(0)}{\tilde{\Delta}_{\parallel}'(0^+)^2} = 0.71 \pm 0.09$ . Increasing the fit range to  $w \in [0, 1.6]$  this value increases to  $0.76 \pm 0.06$ . We thus estimate the scale-free universal ratio to be

$$\frac{\Delta_{\parallel}(0)\Delta_{\parallel}''(0)}{\Delta_{\parallel}'(0^+)^2} \equiv \frac{\tilde{\Delta}_{\parallel}(0)\tilde{\Delta}_{\parallel}''(0)}{\tilde{\Delta}_{\parallel}'(0^+)^2} = 0.74 \pm 0.07. \quad (85)$$

This is larger than the one-loop value of  $\frac{2}{3}$  predicted in Ref. [61]. It is fairly close to the value of 0.73(3) measured experimentally in two-dimensional magnetic domain walls [59]. It can also be compared to the value predicted by FRG for short-range elasticity in the  $N = 1$  case [28,59], where one gets  $\frac{2}{3}$  in  $d = 4$  (exact), 0.71 in  $d = 3$  (two-loop), 0.75 in  $d = 2$  (two-loop), 0.79 in  $d = 1$  (two-loop), and 0.822 (toy model in  $d = 0$ ). Within error bars the value of Eq. (85) agrees with the one predicted by the theory for  $N = 1$ , and thus confirms the planar approximation.

In Fig. 10(b) we show that the correlator  $\Delta_{\perp} \equiv \Delta_{\perp,\perp}$  can, for different  $m$ , fairly well be collapsed, within the statistical error bars, using a master curve  $\Delta_{\perp}(w) = m^2 \tilde{\Delta}_{\perp}(wm^2)$ , as

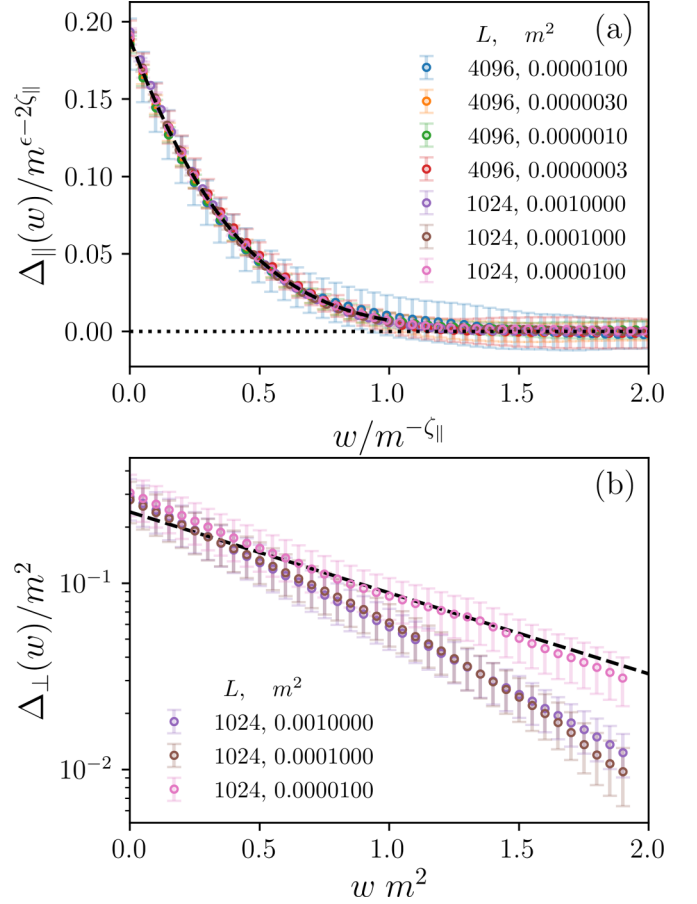


FIG. 10. (a) Scaled force-force correlator for components in the parallel direction (with  $\epsilon = 4 - d = 3$ ). The dashed line corresponds to a fit of  $f(x) = ce^{-ax-bx^2-dx^3}$ , yielding  $a = 2.38 \pm 0.07$ ,  $b = 0.8 \pm 0.2$ ,  $c = 0.188 \pm 0.001$ , and  $d = 0.09 \pm 0.21$ . (b) Scaled force-force correlator for components in the perpendicular direction. The dashed line corresponds to a fit to  $g(x) = a' \exp(-x)$ ,  $a' = 0.27 \pm 0.02$ .

anticipated in Eq. (43). By fitting the predicted exponential decay as  $\tilde{\Delta}_{\perp}(w) = \sigma \exp(-dw)$  for all curves combined, we obtain  $\sigma = 0.306 \pm 0.027$ ,  $d = 1.50 \pm 0.25$ . The value of  $\sigma$  is fairly close to the single-monomer standard deviation of perpendicular jumps, while the decay constant  $d$  comes out larger. However, we see that reducing  $m$ , the scaling function  $\tilde{\Delta}(w)$  converges more and more to  $\tilde{\Delta}_{\perp}(w) = \sigma e^{-w}$  predicted in Eq. (43). The latter curve is shown in black dashed on Fig. 10(b). It seems convergence is slow, and the prediction (43) is reached only asymptotically. We may therefore suspect that the amplitude ratio (85) has also not yet converged. We defer an in-depth analysis to future work.

### F. Crossover to the fast-flow regime

At finite velocities just above the depinning threshold, the steady-state correlation length is expected to diverge as  $\xi_f \sim (f - f_c)^{-\nu} \sim v^{-\nu/\beta}$ . As for interfaces [88],  $\xi_f$  is a characteristic geometrical crossover length. In Fig. 11(a) we show that for intermediate and large length scales, and different small steady-state velocities

$$S_{\parallel}(q) \sim q^{-(d+2\zeta_{\parallel})} \tilde{S}_{\parallel}(qv^{-\nu/\beta}). \quad (86)$$

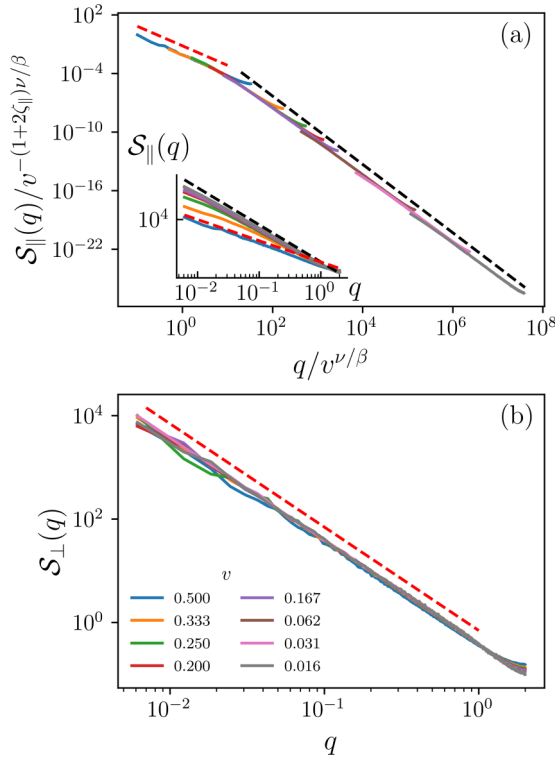


FIG. 11. Steady-state structure factors at finite imposed velocities for  $L = 1024$  and  $m^2 = 0.00001$  for the longitudinal (a) and transversal directions (b). (a) Rescaled structure in the parallel direction. Red dashed lines indicate the fast-flow roughness exponent  $\zeta_{\text{ff}} = \frac{1}{2}$ , and the black dashed lines the depinning roughness exponent  $\zeta_{\parallel} = 1.25$ . The crossover between the two regimes occurs at the depinning correlation length  $\xi_f \sim v^{-\nu/\beta}$ . Inset shows raw nonscaled data. (b) The transverse structure factor appears to be independent of the imposed velocity and described by a roughness exponent  $\zeta_{\perp} = 0.5$  (red dashed line).

Here  $\tilde{\mathcal{S}}_{\parallel}(x) = \text{const}$  for  $x \gg 1$ , while for  $x \ll 1$  one has  $\tilde{\mathcal{S}}_{\parallel}(x) \sim x^{2(\zeta_{\parallel} - \zeta_{\text{EW}})}$ , where  $\zeta_{\text{EW}} = (2 - d)/2$  and  $\zeta_{\parallel} = 1.25$  as given by Eq. (58). From the renormalization-group viewpoint, this result is in agreement with the crossover of the depinning fixed point towards an Edwards-Wilkinson regime, as predicted for the FL [61] and for the interface [32]. In other words, aside from renormalizing the friction such that  $v \sim (f - f_c)^\beta$ , pinning forces on the coarse-grained FL above  $\xi_f$  are similar to thermal noise. What was derived for  $N = 1$  remains valid in the planar approximation.

In Fig. 11(b) we show the structure factor in the perpendicular direction for different velocities near the depinning threshold. Remarkably, there are no signatures of the correlation length  $\xi_f \sim v^{-\nu/\beta}$ . That is, for nonmicroscopic length scales we find that

$$S_{\perp}(q) \sim q^{-(1+2\zeta_{\perp})} \sim q^{-2}, \quad (87)$$

and we are not able to detect any geometrical crossover at  $\xi_f(v)$ , at variance with the clear crossover observed in  $S_{\parallel}(q)$ . The reason is that the assumptions entering Eq. (37) remain unchanged for large driving velocities  $v$ . We thus only observe a crossover imposed by the confining potential at  $q\xi_m \approx 1$ . At large velocities, in the *fast-flow regime*, the depinning correla-

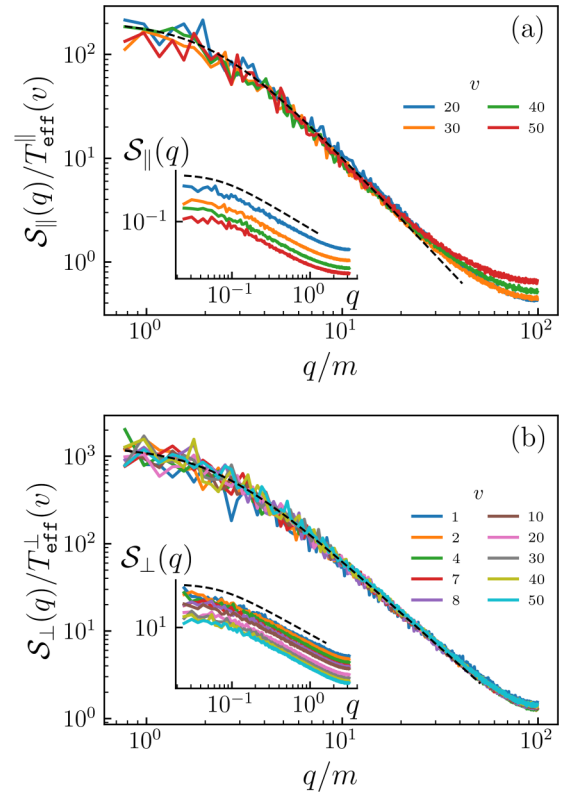


FIG. 12. Rescaled structure factors at different large velocities for  $m^2 = 0.001$  and  $L = 1024$  in the longitudinal (a) and transverse (b) directions. In both cases, raw data (insets) can be collapsed by using effective temperatures  $T_{\text{eff}}^{\parallel}(v)$  (a) and  $T_{\text{eff}}^{\perp}(v)$  (b). Dashed lines correspond to the purely “thermal”  $\sim (cq^2 + m^2)^{-1}$  dependence.

tion length becomes small and it is expected that the pinning forces became a rapidly fluctuating uncorrelated noise acting on an otherwise flat moving elastic FL. We hence expect  $\mathcal{S}_{\alpha}(q) \sim (cq^2 + m^2)^{-1}$  at intermediate scales,  $q\xi_m = q/m > 1$ , and a crossover towards  $\mathcal{S}_{\alpha}(q) \sim \text{const}$  for  $q\xi_m = q/m < 1$ . In the insets of Fig. 12 we verify this by showing the structure factor as a function of  $v$  (not necessarily small), for the longitudinal and perpendicular directions. At variance to small  $v$ ,  $S_{\perp}(q)(cq^2 + m^2)$  is  $v$  dependent. Its behavior at small  $q$  motivates the study of effective temperatures. These are introduced from generalized fluctuation-dissipation theorems by using that the static linear response function in the  $\alpha$  direction due to an external time-independent but  $q$ -dependent field in the  $\alpha'$  direction is *exactly* given by

$$\chi_{\alpha,\alpha'} = \delta_{\alpha,\alpha'} \chi(q) \equiv \frac{\delta_{\alpha,\alpha'}}{cq^2 + m^2}, \quad (88)$$

due to the statistical tilt symmetry [30]. In equilibrium ( $v = 0$ ) at a finite temperature  $T$ , the fluctuation-dissipation theorem implies that  $\mathcal{S}_{\alpha}(q) = T\chi(q)$ . For the driven, out-of-equilibrium FL at zero temperature we can thus define anisotropic effective temperatures  $T_{\text{eff}}^{\alpha}$  ( $\alpha = \parallel, \perp$ ):

$$T_{\text{eff}}^{\alpha}(v) := \frac{\mathcal{S}_{\alpha}(q)}{\chi(q)} = (cq^2 + m^2)\mathcal{S}_{\alpha}(q). \quad (89)$$

At large scales compared to the correlation length  $\xi_f(v)$ , and since  $\mathcal{S}_{\alpha}(q) \sim (cq^2 + m^2)^{-1}$ , a single anisotropic effective

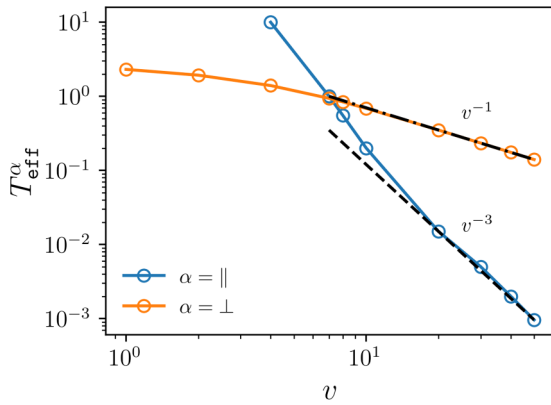


FIG. 13. Effective temperatures as a function of the velocity for  $m^2 = 0.001$  and  $L = 1024$ . Dashed lines indicate asymptotic dependencies.

temperature is sufficient for the whole regime. This is expected to hold for  $2\pi\xi_f^{-1} \gg q$ . It remains valid for the largest length scales, and when  $q < m$ , there is a crossover to a flat regime  $S_\alpha(q) \simeq T_{\text{eff}}(v)m^{-2}$ , due to the confining potential. Therefore,  $S_\alpha(q)/T_{\text{eff}}^\alpha$  is independent of  $v$  for large length scales (small  $q$ ) as shown in Fig. 12, and  $T_{\text{eff}}^\alpha(v)$  describes large-scale fluctuations in general.

Since large length scales are associated with a slow dynamics, these definitions may yield a *bona fide* temperature in a thermodynamic sense [89]. Using these definitions in the main panels of Fig. 12 we show that  $S_\alpha(q)$  for different velocities  $v$  can be distinguished by  $T_{\text{eff}}^\alpha(v)$  for small enough  $q$ . For large  $q$ , only the parallel direction shows a deviation from the master curve, indicating that the parallel direction retains genuine nonequilibrium features at short length scales.

The velocity dependence of the two effective temperatures is shown in Fig. 13. They are direction dependent, and monotonously decrease with increasing  $v$ . They intersect at a characteristic velocity of  $v \approx 7$ , above which  $T_{\text{eff}}^\perp > T_{\text{eff}}^\parallel$ . At small  $v$  the transversal temperature  $T_{\text{eff}}^\perp$  saturates at  $T_{\text{eff}}^\perp = \sigma \approx \frac{1}{3}$ , as discussed above, explaining why on Fig. 11(b) no appreciable velocity dependence is observed. The observed asymptotic forms are  $T_{\text{eff}}^\parallel \sim v^{-3}$  and  $T_{\text{eff}}^\perp \sim v^{-1}$ .

The two-component Edwards-Wilkinson type of scaling with effective temperatures  $T_{\text{eff}}^\alpha$  of the structure factor at large velocities implies that the global width scales as

$$W_\alpha^2 \sim \frac{T_{\text{eff}}^\alpha}{m^{2\zeta_{\text{EW}}}} = \frac{T_{\text{eff}}^\alpha}{m}, \quad (90)$$

as verified in Fig. 14 for each direction, as a function of velocity.

The crossing of the effective temperatures is associated with the existence of an isotropic point for the global width, above which the FL tends to be elongated in the transverse direction, in contrast with the situation near depinning where they are elongated in the longitudinal direction. This was predicted in Ref. [16] from general arguments. To see this better, it is useful to compute the joint distribution function (13) of local displacements, which gives us a top view of the FL fluctuations in the comoving frame. In the inset of Fig. 14 we do not only see the change of aspect ratio and the reduction of the global width with increasing  $v$ , but we also observe

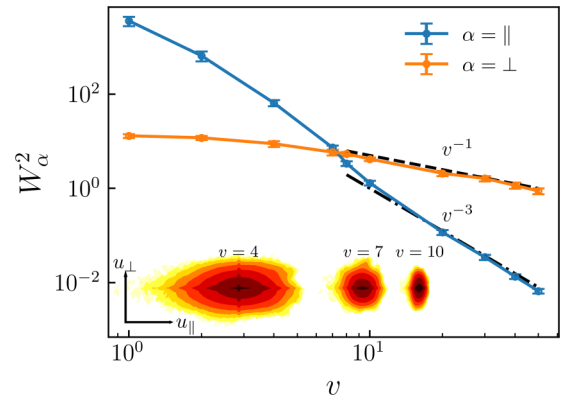


FIG. 14. Mean quadratic widths as a function of the velocity for  $m^2 = 0.001$  and  $L = 1024$ . Dashed lines indicate asymptotic dependencies.

that the parallel-displacement distribution is asymmetric, with a more elongated tail at smaller velocities, in contrast to the symmetric distribution in the perpendicular direction. To characterize it we show in Fig. 15 the reduced distributions of Eq. (12) for a large range of velocities. Only for large  $v$  do they converge towards a Gaussian, as can be seen in the inset of Fig. 15(a): At low velocities (lighter colors) the distribution has asymmetric tails. As shown in the main panel the variance is controlled by the velocity-dependent effective temperatures of Fig. 13. These displacements translate into an appreciable skewness. In Fig. 16 we show the skewness, as a function of

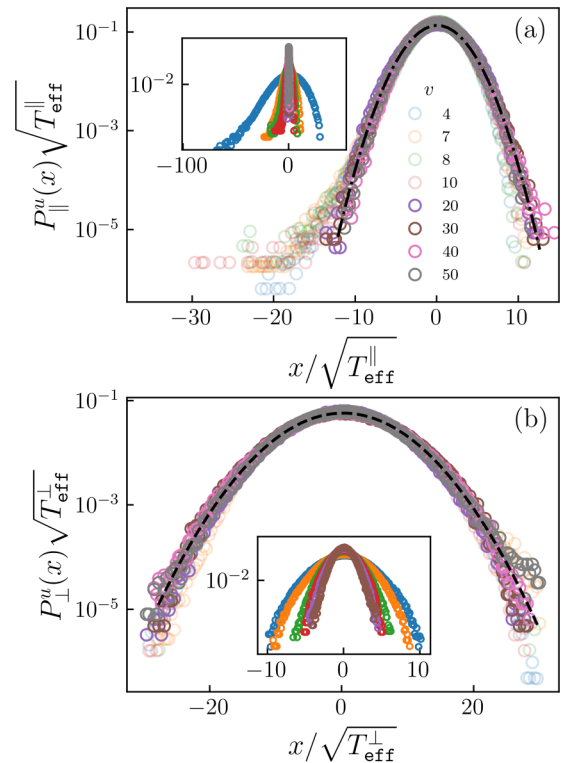


FIG. 15. Local displacement fluctuations around the center of mass in the parallel (a) and perpendicular directions (b). Lighter symbols are used for smaller velocities. Parameters of the simulations are  $m^2 = 0.001$  and  $L = 1024$ . Dashed lines are Gaussian fits.

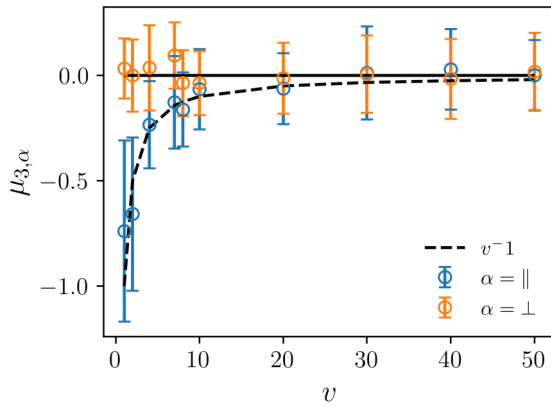


FIG. 16. Skewness of the two components of the local displacement distribution as a function of the velocity for  $m^2 = 0.001$  and  $L = 1024$ .

the velocity, defined as

$$\mu_{3,\alpha} = \frac{\langle [u(x,t) - u_\alpha(t)]^3 \rangle}{W_\alpha^2(t)^{3/2}}. \quad (91)$$

As expected, the perpendicular direction has an undetectable skewness while the longitudinal one presents a negative skewness at small  $v$ . It roughly vanishes as  $\sim 1/v$  for large velocities. In Fig. 17 we also show the kurtosis

$$k_\alpha = \frac{\langle [u(x,t) - u_\alpha(t)]^4 \rangle}{W_\alpha^4(t)}. \quad (92)$$

Within error bars we find  $k_{||} \approx 3$  and  $k_{\perp} \approx 3$  at large velocities, consistent with an approximately Gaussian shape. Only in the longitudinal direction at low velocities we observe a departure from Gaussian,  $k_{||} > 3$ , though with a large error bar.

The above observations are a strong indication for the existence of a *large-deviation* function, encountered for depinning already in Ref. [90]. Provided the limit exists, the large-deviation function  $F(x)$  is defined as

$$F(x) := - \lim_{v \rightarrow \infty} \frac{\ln P(xv)}{v}. \quad (93)$$

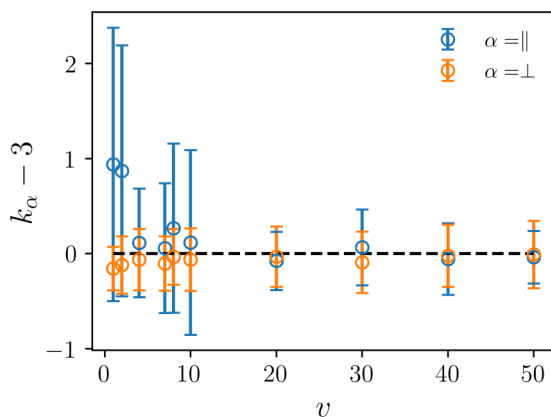


FIG. 17. Kurtosis of the local displacement fluctuations in both directions. The dashed line corresponds to a pure Gaussian.

Since our data do not allow to evaluate  $F(x)$  precisely enough, we leave its determination for future work.

On the other hand, the inset of Fig. 15(b) shows that the perpendicular fluctuations are well approximated by a Gaussian with a velocity-controlled variance

$$P_{\perp}^u(x) \sim e^{-\frac{(x-u_{\perp})^2}{2W_{\perp}^2(v)}}. \quad (94)$$

Since  $W_{\perp}^2(v) \approx T_{\text{eff}}^{\perp}(v)/m$  [see Eq. (90)], the velocity dependence is exclusively controlled by the transverse effective temperature, as shown by the rescaled curves in the main panel of Fig. 15(b). These results show that the perpendicular direction can be described by an Edwards-Wilkinson equation with an effective temperature at all velocities. The longitudinal direction shows genuine nonequilibrium effects well beyond the depinning transition, which disappear roughly as  $1/v$  for large  $v$ .

It is worth noting that these rare asymmetric parallel fluctuations may be more pronounced for strong pinning. For instance, when pinned by nanoparticles, the FL appears as a sequence of convex arcs in the direction of motion connecting localized pinned pieces [62], explicitly breaking the  $\delta u_{||}(z,t) \rightarrow -\delta u_{||}(z,t)$  symmetry. This symmetry is, however, always broken at depinning [28,91]. This kind of structure may explain both tails of the displacement distribution. Nevertheless, at very large velocities both directions display anisotropic Gaussian fluctuations. As discussed in the next section, the anisotropy of these fluctuations is rather sensible to whether the microscopic disorder is RB or RF.

### G. Random-field disorder

So far we discussed RB disorder acting on a vortex line, corresponding to short-range correlated pinning potentials. This type of disorder seems to be the only one relevant in experiments, and in particular for point disorder in bulk superconductors. While we do not know how to realize isotropic RF disorder corresponding to uncorrelated pinning forces, we nevertheless consider it here for comparison. We remind that the two types of disorder are differentiated by their correlators (see Sec. II A).

We first discuss the low-velocity regime near the depinning transition. In Fig. 18(a) we show, using the same exponents of Table I obtained for the RB case, that the steady-state structure factor scales as  $\mathcal{S}_{||}(q) \sim q^{-(1+2\zeta_{||})} G(q\xi)$ ,  $\xi \sim (f - f_c)^{-\nu}$ , with  $G(x) \sim x^{1+2\zeta_{||}}$  for  $x \gg 1$ , and  $G(x) \sim \text{const}$  for  $x \ll 1$ , provided  $\xi < 1/m$  and  $q > m$ . Since the same scaling was shown in Fig. 11(a) for the RB case, this result is again consistent with the planar approximation, and with the finding that RB and RF share the same depinning universality class [35,36]. In Fig. 18(b) we show that  $\mathcal{S}_{\perp}(q) \sim q^{-(1+2\zeta_{\perp})}$ , with no clear signature of  $\xi$ , as observed before in Fig. 11(b) for the RB case.

The crossover to the fast-flow regime reveals some important differences between RB and RF. In Fig. 19 we show that effective temperatures in both directions are well defined and rescale the structure factor for an extended range of velocities. This result can be compared directly to Fig. 12 for the RB case.

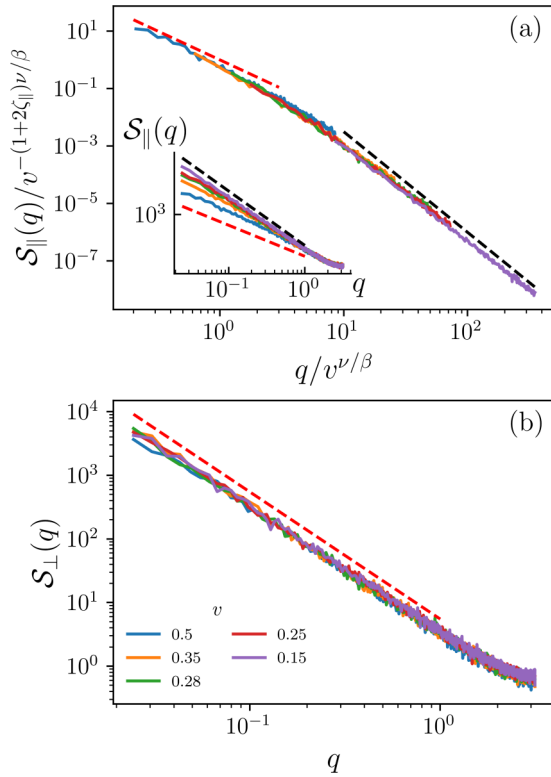


FIG. 18. Steady-state structure factor at low velocities in the parallel (a) and perpendicular (b) directions for RF disorder. (a) The inset shows raw data and the main panel the scaled structure factor in the parallel direction using the exponents obtained for RB disorder. (b) Raw data in the perpendicular direction appear to be independent of  $v$ . See Fig. 11 for a direct comparison with the RB case.

In Figs. 20 and 21 for the anisotropic effective temperatures and global widths we see that at intermediate velocities the RF case is qualitatively similar to the RB case, in the sense that  $T_{\text{eff}}^{\parallel} > T_{\text{eff}}^{\perp}$  and  $W_{\parallel}^2 > W_{\perp}^2 \sim 1/v$ . For small velocities, the local displacement distribution is asymmetric in the longitudinal direction, as was shown in Fig. 15 for the RB case. In contrast, for larger velocities the curves for the different directions no longer cross at a characteristic velocity (see Figs. 20 and 21), but directly merge into an isotropic decay at large velocities, with  $T_{\text{eff}}^{\parallel} \approx T_{\text{eff}}^{\perp} \sim 1/v$  and  $W_{\parallel}^2 \approx W_{\perp}^2 \sim 1/v$ . Isotropic RF disorder thus produces isotropic fluctuations at large velocities,

TABLE I. Critical depinning exponents obtained in this work. We also indicate the figure where the exponent was fitted or tested and the scaling relations that hold within our numerical uncertainty. The same exponents and relations hold both for RB and RF disorder.

$\zeta_{\parallel}$	$1.25 \pm 0.01$	Fig. 3(a)	
$\zeta_{\perp}$	$0.5 \pm 0.01$	Fig. 3(b)	
$z_{\parallel}$	$1.43 \pm 0.01$	Fig. 4(a)	
$z_{\perp}$	$2.27 \pm 0.05$	Fig. 4(a)	$z_{\perp} = z_{\parallel} + 1/v$
$\nu$	$1.33 \pm 0.02$	Fig. 11(a)	$\nu = 1/(2 - \zeta_{\parallel})$
$\beta$	$0.24 \pm 0.01$	Fig. 4(b)	$\beta = \nu(z_{\parallel} - \zeta_{\parallel})$
$\tau_{\parallel}$	$1.09 \pm 0.03$	Fig. 7(a)	$\tau_{\parallel} = 2 - 2/(1 + \zeta_{\parallel})$
$\tau_{\perp}$	$1.17 \pm 0.06$	Fig. 7(b)	$\tau_{\perp} = 2\tau_{\parallel} - 1$

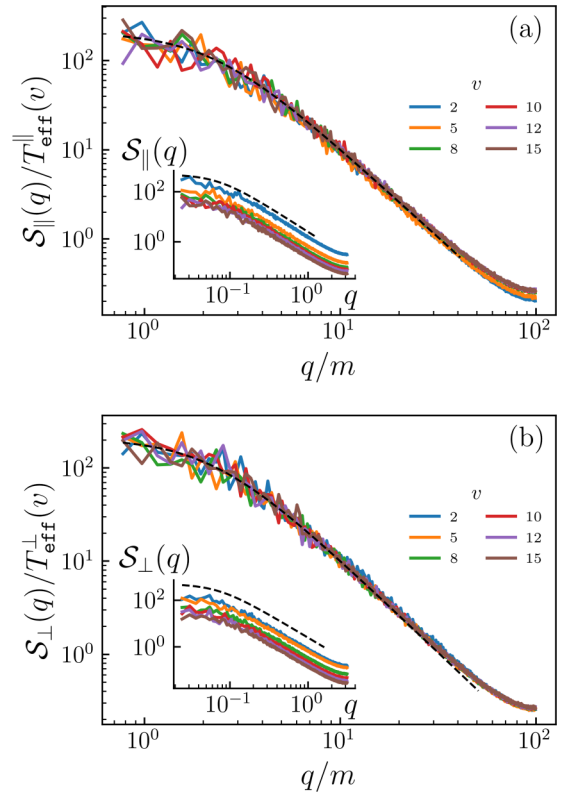


FIG. 19. Rescaled structure factors at different (large) velocities for  $m^2 = 0.001$  and  $L = 1024$  in the longitudinal (a) and transverse (b) directions, for RF disorder. In both cases, raw data (insets) can be collapsed by using the effective temperatures  $T_{\text{eff}}^{\parallel}(v)$  (a) and  $T_{\text{eff}}^{\perp}(v)$  (b). Dashed lines correspond to a purely “thermal”  $\sim (cq^2 + m^2)^{-1}$  dependence. See Fig. 12 for a comparison to the RB case.

ities, in contrast with the anisotropic fluctuations in the RB case.

## V. DISCUSSION AND CONCLUSIONS

We studied depinning and flow of a flux lines with harmonic elasticity in an isotropic random medium with

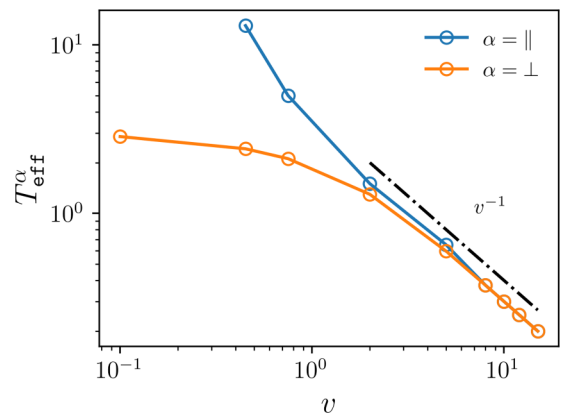


FIG. 20. Effective temperatures as a function of the mean velocity for RF disorder. Dashed-dotted lines indicate the asymptotic behavior.

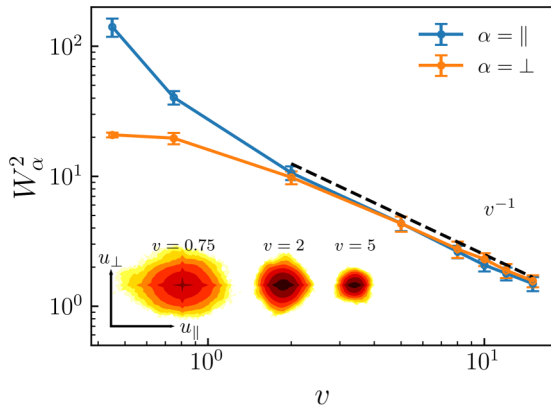


FIG. 21. Mean-squared widths as a function of mean velocity for RF disorder. Dashed-dotted lines indicate the asymptotic behavior. The inset displays the joint local-displacement distribution for three velocities.

short-range correlated disorder. We report phenomena, such as the asymmetry of local parallel displacements at low velocities, the inversion of the aspect ratio of widths in the RB case, and important differences between RB and RF in the fast-flow regime.

For quasistatic driving we calculated several universal quantities. In Table I we summarize the values of all critical exponents that we measured, and the relations between them according to our numerical tests. Some critical exponents differ appreciably from previous reports. Our value  $\beta = 0.24(1)$  differs from  $\beta \approx 0.31$  or  $\beta = 0$  given in Ref. [61], but is indistinguishable from the one for interfaces in two-dimensional random media [2]. The value  $\zeta_{\parallel} \approx 1.25(1)$  contrasts with  $\zeta_{\parallel} = 1$  from Ref. [61], agrees with the one reported in Ref. [62] for strong disorder, and is indistinguishable from the one for one-dimensional interfaces [2,38,40]. This result is physically relevant as  $\zeta_{\parallel} > 1$  implies the breakdown of linear elasticity at large length scales. Some proposed scaling relations do not pass our numerical tests, particularly  $\zeta_{\perp} = \zeta_{\parallel} - 1/2$  [61] and  $\zeta_{\perp} = 5\zeta_{\parallel}/2 - 2$  [26]. Other relations predicted in Ref. [61] are verified, as shown in Table I. We added the tested relation for  $\tau_{\parallel}$ , which is identical to the one for interfaces in two dimensions [30,84]. A relation links  $\tau_{\perp}$  to  $\tau_{\parallel}$ . In spite of differences in the above scaling relations, the main message is that the Ertas-Kardar planar approximation is working well, provided we use the appropriate results for the  $(D, N) = (1, 1)$  case [42], and correct the roughness exponent for the transversal direction to  $\zeta_{\perp} = (2 - d)/2$ . We explicitly verified that for  $(D, N) = (1, 2)$ , microscopic RB and RF disorder lead to a single RF universality class at depinning, a result we expect from the planar approximation.

As for  $N = 1$ , one can expect that the breakdown of linear elasticity we report for  $N = 2$  may be avoided if we add extra terms to the model of Eq. (5). Introducing anisotropy [49] or anharmonic corrections to the elasticity [53] for  $N = 1$  are known to change the quenched Edwards-Wilkinson to the quenched Kardar-Parisi-Zhang (KPZ) (or directed-percolation) depinning universality class. In the low-wavelength limit this amounts to adding a KPZ term of the form  $\lambda(\partial_x u)^2$  to the quenched Edwards-Wilkinson equation.

As a consequence, the statistical tilt symmetry is broken, elasticity renormalizes, and the roughness exponent reduces to  $\zeta \approx 0.63$ , bounding fluctuations for large distances.

Modifying accordingly the equations for  $N = 2$  is more complex. We expect that if the planar approximation still works, adding nonlinear elasticity also reduces the roughness exponent to  $\zeta_{\parallel} = 0.63$ ,  $\zeta_{\perp} = 0.5$ , as for  $N = 1$ . The description in terms of a KPZ term is more intricate since the latter has one more field  $u_{\alpha}$ , i.e., one more index. The additional term in  $\partial_t u_{\alpha}$  is of the form  $\lambda_{\alpha}^{\beta\gamma} \partial_x u_{\beta} \partial_x u_{\gamma}$ . This leaves open the possibility for different tensorial structures and universality classes.

EK [61] argued that anisotropy would lead to  $\zeta_{\parallel} \approx 0.63$ , if a tilt is not imposed and to  $\zeta_{\parallel} \approx 0.5$ , if a tilt is imposed, while  $\zeta_{\perp}$  and  $z_{\perp}$  may take different values depending on the remaining symmetries. It would be interesting to check these predictions and to find the possible new universality classes.

For intermediate driving velocities we show that the transverse local fluctuations are Gaussian, and that the structure of the elastic string is described by a single exponent  $\zeta_{\perp} = \frac{1}{2}$ , together with a well-defined effective temperature that tends to saturate at small velocities and vanishes as  $T_{\text{eff}}^{\perp} \sim 1/v$  at large velocities. This supports the identification of a transverse “shaking temperature” in Ref. [16] as a limit of the transverse effective temperature we define, and which is valid for all finite velocities. Local longitudinal fluctuations are skewed at low velocities and become Gaussian at large ones, with an effective longitudinal temperature vanishing as  $T_{\text{eff}}^{\parallel} \sim 1/v^3$  for RB disorder. At large velocities the correlation length becomes small and the interface is essentially flat in the driving direction (see Fig. 14). This result is inconsistent with the prediction of a zero “longitudinal shaking temperature” in Ref. [16]. The difference may be attributed to the fact that the latter calculation neglects terms of order  $O(1/v^2)$  and for RB disorder only contains the leading term proportional to  $\int_u \Delta(u) = 0$ . On the other hand, the  $1/v^3$  behavior is inconsistent with the prediction of an “Edwards-Wilkinson temperature” proportional to  $1/v$  [32], if we assume that the planar approximation holds in this regime. This discrepancy is due to the use of a  $v$ -independent RF disorder in the high-velocity regime, ignoring that the microscopic disorder is RB, and that the driving velocity reduces the effects of the RG flow bringing it to RF. In contrast, we confirmed numerically the analytical expectation that microscopic RF disorder produces an isotropic effective temperature vanishing as  $T_{\text{eff}}^{\parallel} \approx T_{\text{eff}}^{\perp} \sim 1/v$ . The same dependencies in the effective temperatures are observed in the diffusion of a single monomer driven in two-dimensional RB disorder [73]. This suggests that the longitudinal effective temperature in the large-velocity regime is controlled by what happens for a single monomer. We confirm that in the comoving frame the string can be described as a two-component Edwards-Wilkinson line with uncorrelated noise controlled by  $v$  as predicted in [16,32], with an anisotropy that depends as discussed on the microscopic disorder. These results show that the nature of the microscopic disorder can be detected by observing the anisotropic fluctuations in the fast-flow regime.

Our results should be relevant for flux lines or other elastic lines in random media, such as polymers driven in random



quenched media, or cracks. Since cracks have long-range elasticity, we expect the transversal roughness to be logarithmic. This agrees with [92], and was experimentally observed in [93].

### ACKNOWLEDGMENTS

We thank L. Ponsón for discussions. We acknowledge financial support through Grants No. PICT 2016-0069, No. PICT-2019-01991, and No. SIIP-Uncuyo 06/C578. This work used computational resources from CCAD–Universidad Nacional de Córdoba, and from the Physics Department–Centro Atómico Bariloche, both of which are part of SNCAD–MinCyT, Republic Argentina.

### APPENDIX A: FORCE-CONTROLLED DRIVING VERSUS VELOCITY-CONTROLLED DRIVING

Using the velocity-controlled driving we performed a set of simulations for different masses and velocities. In Fig. 11 we show the depinning transition with exponents  $\zeta_{\parallel} = 1.25$ ,  $\nu = 1.33$ , and  $\beta = 0.33$ . The critical force fluctuates around  $f_c(m) = m^2 \langle vt - u_{\parallel} \rangle$ , and this scales with the mass as  $f_c(m) \approx m^2 u_m = m^{2-\zeta_{\parallel}}$  as shown in Fig. 22. Fitting this relation, we extract the zero-mass critical force  $f_c(0) = 0.77321(5)$ .

With the same parameters we perform a set of simulations in the force-controlled driving ensemble. In Fig. 23 we show the structure factor for the parallel direction scaled according to the depinning length  $l_{\parallel} \sim v(f)^{-\frac{\nu}{\beta}} = (f - f_c)^{-\nu}$  with the same scaling exponents  $\zeta_{\parallel}$ ,  $\nu$  and critical force  $f_c = 0.7656$ . The distance to the zero-mass critical force is  $|f_c(0) - f_c| \approx 0.0076$ .

### APPENDIX B: CORRELATIONS OF AN ORNSTEIN-UHLENBECK PROCESS

We wrote the equation of motion

$$\partial_{u_{\parallel}} u_{\perp}(x, u_{\parallel}) = -m^2 u_{\perp}(x, u_{\parallel}) + \nabla^2 u_{\perp}(x, u_{\parallel}) + \sqrt{2\sigma} \eta(x, t), \quad (\text{B1})$$

$$\langle \eta(x, u_{\parallel}) \eta(x', u'_{\parallel}) \rangle = \delta^d(x - x') \delta(u_{\parallel} - u'_{\parallel}). \quad (\text{B2})$$

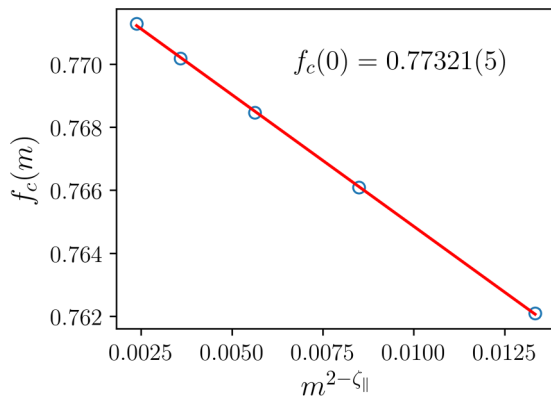


FIG. 22. Critical force as a function of mass behaves as  $f_c(m) \sim m^2 u_m = m^{2-\zeta_{\parallel}}$ . Extrapolated to  $m = 0$  it gives the zero-mass critical force  $f_c(0) = 0.77321(5)$ .

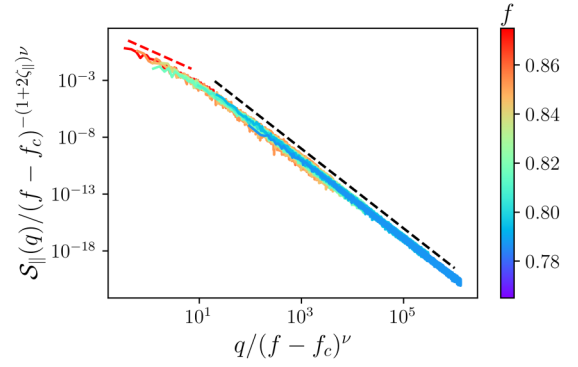


FIG. 23. Scaled steady-state structure factor for the constant-force ensemble according to the depinning length  $l_{\parallel} \sim v(f)^{-\frac{\nu}{\beta}} = [f - f_c(0)]^{-\nu}$  with  $\zeta_{\parallel} = 1.25$ ,  $\nu = 1.33$  and zero-mass critical force  $f_c(0) = 0.77321(5)$ . Red dashed lines indicate the fast-flow roughness exponent  $\zeta_{\text{ff}} = 0.5$ , and the black dashed lines the depinning roughness exponent  $\zeta_{\parallel} = 1.25$ .

Integrating over  $x$ , dividing by  $L^d$ , and replacing  $u_{\parallel} \rightarrow w$  yields

$$\partial_w u_{\perp}(w) = -m^2 u_{\perp}(w) + \sqrt{\frac{2\sigma}{L^d}} \eta(w), \quad (\text{B3})$$

$$\langle \eta(w) \eta(w') \rangle = \delta(w - w'). \quad (\text{B4})$$

This is an Ornstein-Uhlenbeck process, solved by

$$u_{\perp}(w) = \int_{-\infty}^w dw_1 e^{-m^2(w-w_1)} \xi(w_1). \quad (\text{B5})$$

It leads to force correlations

$$\begin{aligned} \Delta_{\perp}(w - w') &= m^4 L^d \langle u_{\perp}(w) u_{\perp}(w') \rangle \\ &= m^4 L^d \int_{-\infty}^w dw_1 \int_{-\infty}^{w'} dw_2 e^{-m^2(w+w'-w_1-w_2)} \langle \eta(w_1) \eta(w_2) \rangle \\ &= 2\sigma m^4 \int_{-\infty}^{\min(w, w')} d\tilde{w} e^{-m^2(w+w'-2\tilde{w})} \\ &= \sigma m^2 e^{-m^2|w-w'|}. \end{aligned} \quad (\text{B6})$$

### APPENDIX C: SINGLE-MONOMER DIFFUSION IN THE COMOVING FRAME

Let us consider an overdamped particle driven by a force  $f$  in a one-dimensional space with quenched random forces:

$$\eta \dot{x} = F(x) + f, \quad (\text{C1})$$

where  $F(x)$  is a short-range correlated quenched random force field such that

$$\overline{F(x)} = 0, \quad (\text{C2})$$

$$\overline{F(x)F(x')} = f_0^2 g(|x - x'|/d_0). \quad (\text{C3})$$

Here,  $d_0$  is a characteristic length,  $f_0$  a characteristic force amplitude, and  $g(u)$  a rapidly decaying function of unit range and unit amplitude. Without loss of generality we can adimensionalize the equation of motion by measuring distances in units of  $d_0$ , forces in units of  $f_0$ , and time in units of

$\tau_0 = \eta d_0 / f_0$ , such that

$$\dot{x} = F(x) + f. \quad (\text{C4})$$

We consider two toy models, one for RF and one for RB disorder, in which the force fields are piecewise constant.

### 1. RF disorder

To construct a RF disorder such that  $\int_y g(y) > 0$  we take

$$F(x) = R_{[x]}, \quad (\text{C5})$$

where  $[\dots]$  denotes the integer part. The  $R_n$  are uniformly distributed random numbers in the interval  $[-1, 1]$  such that

$$\overline{R_n R_m} = \frac{\delta_{n,m}}{3}. \quad (\text{C6})$$

From Eq. (C4) the time spent in the interval  $n$  is

$$\Delta t_n = \frac{1}{R + f}, \quad (\text{C7})$$

where  $R \equiv R_n$ , and hence

$$\langle \Delta t \rangle = \frac{1}{2} \int_{-1}^1 \frac{1}{R + f} dR = \frac{1}{2} \ln \left( \frac{f+1}{f-1} \right), \quad (\text{C8})$$

$$\langle \Delta t^2 \rangle = \frac{1}{2} \int_{-1}^1 \frac{1}{(R + f)^2} dR = \frac{1}{f^2 - 1}. \quad (\text{C9})$$

The mean velocity is

$$v = \frac{1}{\langle \Delta t \rangle} = \frac{2}{\ln \left( \frac{f+1}{f-1} \right)}, \quad (\text{C10})$$

displaying a depinning transition at  $f = 1$ , while for  $f \gg 1$ ,  $v \simeq f$  as expected. The (differential) mobility is

$$\mu := \frac{dv}{df} = \frac{4}{(f^2 - 1) \ln \left( \frac{f+1}{f-1} \right)^2}, \quad (\text{C11})$$

such that  $\mu \rightarrow \infty$  when  $f \rightarrow 1$  and  $\mu \rightarrow 1$  when  $f \rightarrow \infty$ . The diffusion constant in the comoving frame is  $D \equiv \langle [x - vt]^2 \rangle / t = \langle [1 - v\Delta t]^2 \rangle$  and can be expressed in terms of  $\langle \Delta t \rangle$

and  $\langle \Delta t^2 \rangle$  as

$$D = \frac{\langle \Delta t^2 \rangle - \langle \Delta t \rangle^2}{\langle \Delta t \rangle^3}. \quad (\text{C12})$$

Using the generalized Einstein relation we get the effective temperature as  $T_{\text{eff}} = D/\mu$ .

We are interested in the  $f \gg 1$  fast-flow behavior of  $D$  and  $T_{\text{eff}}$ . Expanding in powers of  $1/f$  we get

$$D \simeq \frac{1}{3f} + \frac{7}{45f^3} + O(f^{-5}), \quad (\text{C13})$$

$$T_{\text{eff}} \simeq \frac{1}{3f} + \frac{2}{45f^3} + O(f^{-5}). \quad (\text{C14})$$

Recovering the physical dimensions, we get at the lowest order that  $D \sim (d_0^2/\tau_0)(f_0/f) = (f_0 d_0/\eta)(f_0/f) \sim d_0 v_0^2/v$ , with  $v_0 = f_0/\eta$ .

### 2. RB disorder

To model RB disorder with  $\int_y g(y) = 0$ , we define the random forces in Eq. (C4) as

$$F(x) = R_{[x]} \text{sign}(x - [x] - 1/2) + f. \quad (\text{C15})$$

As above  $R_n$  are independent and identically distributed random variables, uniformly distributed in  $[-1, 1]$ . By repeating the procedure of the previous section we obtain  $\langle \Delta t \rangle$  as for the RF case, and thus identical  $v$  and  $\mu$  as a function of  $f$ . However,  $\langle \Delta t^2 \rangle$  is different:

$$\begin{aligned} \langle \Delta t^2 \rangle &= \frac{1}{2} \int_{-1}^1 \left[ \frac{1}{2(f+R)} + \frac{1}{2(f-R)} \right]^2 dR \\ &= \frac{1}{4f} \left[ \frac{2f}{f^2-1} + \ln \left( \frac{f+1}{f-1} \right) \right]. \end{aligned} \quad (\text{C16})$$

This leads to different asymptotic behaviors,

$$D \simeq T_{\text{eff}} \simeq \frac{4}{45f^3} + O(f^{-5}). \quad (\text{C17})$$

Recovering physical dimensions we get  $D \sim d_0 v_0 (f_0/f)^3 \sim d_0 v_0^4/v^3$ , with  $v_0 = f_0/\eta$ .

- 
- [1] G. Durin and S. Zapperi, The Barkhausen effect, in *The Science of Hysteresis*, edited by G. Bertotti and I. Mayergoyz (Elsevier, Amsterdam, 2006), p. 51.
- [2] J. Ferré, P. Metaxas, A. Mougin, J.-P. Jamet, J. Gorchon, and V. Jeudy, Universal magnetic domain wall dynamics in the presence of weak disorder, *C. R. Phys.* **14**, 651 (2013).
- [3] G. Durin, F. Bohn, M. A. Correa, R. L. Sommer, P. LeDoussal, and K. J. Wiese, Quantitative Scaling of Magnetic Avalanches, *Phys. Rev. Lett.* **117**, 087201 (2016).
- [4] W. Kleemann, Universal domain wall dynamics in disordered ferroic materials, *Annu. Rev. Mater. Res.* **37**, 415 (2007).
- [5] P. Paruch and J. Guyonnet, Nanoscale studies of ferroelectric domain walls as pinned elastic interfaces, *C. R. Phys.* **14**, 667 (2013).
- [6] D. Bonamy, S. Santucci, and L. Ponson, Crackling Dynamics in Material Failure as the Signature of a Self-Organized Dynamic Phase Transition, *Phys. Rev. Lett.* **101**, 045501 (2008).
- [7] L. Ponson, Depinning Transition in the Failure of Inhomogeneous Brittle Materials, *Phys. Rev. Lett.* **103**, 055501 (2009).
- [8] C. Le Priol, J. Chopin, P. Le Doussal, L. Ponson, and A. Rosso, Universal Scaling of the Velocity Field in Crack Front Propagation, *Phys. Rev. Lett.* **124**, 065501 (2020).
- [9] S. Moulinet, A. Rosso, W. Krauth, and E. Rolley, Width distribution of contact lines on a disordered substrate, *Phys. Rev. E* **69**, 035103(R) (2004).
- [10] P. L. Doussal, Sinai model in presence of dilute absorbers, *J. Stat. Mech.* (2009) P07032.
- [11] R. Planet, S. Santucci, and J. Ortín, Avalanches and Non-Gaussian Fluctuations of the Global Velocity of Imbibition Fronts, *Phys. Rev. Lett.* **102**, 094502 (2009).
- [12] S. Atis, A. K. Dubey, D. Salin, L. Talon, P. Le Doussal, and K. J. Wiese, Experimental Evidence for Three Universality Classes for Reaction Fronts in Disordered Flows, *Phys. Rev. Lett.* **114**, 234502 (2015).

- [13] E. Bayart, I. Svetlizky, and J. Fineberg, Fracture mechanics determine the lengths of interface ruptures that mediate frictional motion, *Nat. Phys.* **12**, 166 (2015).
- [14] A. Nicolas, E. E. Ferrero, K. Martens, and J.-L. Barrat, Deformation and flow of amorphous solids: A review of mesoscale elastoplastic models, *Rev. Mod. Phys.* **90**, 045006 (2018).
- [15] J. P. Sethna, M. K. Bierbaum, K. A. Dahmen, C. P. Goodrich, J. R. Greer, L. X. Hayden, J. P. Kent-Dobias, E. D. Lee, D. B. Liarte, X. Ni, K. N. Quinn, A. Raju, D. Z. Rocklin, A. Shekhawat, and S. Zapperi, Deformation of crystals: Connections with statistical physics, *Annu. Rev. Mater. Res.* **47**, 217 (2017).
- [16] T. Nattermann and S. Scheidl, Vortex-glass phases in type-II superconductors, *Adv. Phys.* **49**, 607 (2000).
- [17] T. Giamarchi and S. Bhattacharya, Vortex phases, in *2001 Cargese School on "Trends in High Magnetic Field Science"* (Springer, Berlin, 2002).
- [18] P. Le Doussal, Novel phases of vortices in superconductors, *Int. J. Mod. Phys. B* **24**, 3855 (2010).
- [19] W.-K. Kwok, U. Welp, A. Glatz, A. E. Koshelev, K. J. Kihlstrom, and G. W. Crabtree, Vortices in high-performance high-temperature superconductors, *Rep. Prog. Phys.* **79**, 116501 (2016).
- [20] A. U. Thomann, V. B. Geshkenbein, and G. Blatter, Vortex dynamics in type-II superconductors under strong pinning conditions, *Phys. Rev. B* **96**, 144516 (2017).
- [21] I. A. Sadovskyy, A. E. Koshelev, W.-K. Kwok, U. Welp, and A. Glatz, Targeted evolution of pinning landscapes for large superconducting critical currents, *Proc. Natl. Acad. Sci. USA* **116**, 10291 (2019).
- [22] S. Eley, A. Glatz, and R. Willa, Challenges and transformative opportunities in superconductor vortex physics, *J. Appl. Phys.* **130**, 050901 (2021).
- [23] T. Schulz, R. Ritz, A. Bauer, M. Halder, M. Wagner, C. Franz, C. Pfeleiderer, K. Everschor, M. Garst, and A. Rosch, Emergent electrodynamics of skyrmions in a chiral magnet, *Nat. Phys.* **8**, 301 (2012).
- [24] E. A. Jagla and A. B. Kolton, A mechanism for spatial and temporal earthquake clustering, *J. Geophys. Res. Solid Earth* **115**, B05312 (2010).
- [25] E. A. Jagla, F. P. Landes, and A. Rosso, Viscoelastic Effects in Avalanche Dynamics: A Key to Earthquake Statistics, *Phys. Rev. Lett.* **112**, 174301 (2014).
- [26] M. Kardar, Nonequilibrium dynamics of interfaces and lines, *Phys. Rep.* **301**, 85 (1998).
- [27] D. S. Fisher, Collective transport in random media: From superconductors to earthquakes, *Phys. Rep.* **301**, 113 (1998).
- [28] K. Wiese, Theory and experiments for disordered elastic manifolds, depinning, avalanches, and sandpiles, [arXiv:2102.01215](https://arxiv.org/abs/2102.01215).
- [29] T. Nattermann, S. Stepanow, L.-H. Tang, and H. Leschhorn, Dynamics of interface depinning in a disordered medium, *J. Phys. II (France)* **2**, 1483 (1992).
- [30] O. Narayan and D.S. Fisher, Threshold critical dynamics of driven interfaces in random media, *Phys. Rev. B* **48**, 7030 (1993).
- [31] H. Leschhorn, T. Nattermann, S. Stepanow, and L.-H. Tang, Driven interface depinning in a disordered medium, *Ann. Phys.* **509**, 1 (1997).
- [32] P. Chauve, T. Giamarchi, and P. LeDoussal, Creep and depinning in disordered media, *Phys. Rev. B* **62**, 6241 (2000).
- [33] A. Kolton, S. Bustingorry, E. Ferrero, and A. Rosso, Uniqueness of the thermodynamic limit for driven disordered elastic interfaces, *J. Stat. Mech.* (2013) P12004.
- [34] X. Cao, S. Bouzat, A. B. Kolton, and A. Rosso, Localization of soft modes at the depinning transition, *Phys. Rev. E* **97**, 022118 (2018).
- [35] P. Chauve, P. LeDoussal, and K. Wiese, Renormalization of Pinned Elastic Systems: How does it Work Beyond One Loop? *Phys. Rev. Lett.* **86**, 1785 (2001).
- [36] P. LeDoussal, K. J. Wiese, and P. Chauve, 2-loop functional renormalization group analysis of the depinning transition, *Phys. Rev. B* **66**, 174201 (2002).
- [37] A.A. Fedorenko and S. Stepanow, Universal energy distribution for interfaces in a random-field environment, *Phys. Rev. E* **68**, 056115 (2003).
- [38] H. Leschhorn, Interface depinning in a disordered medium numerical results, *Phys. A (Amsterdam)* **195**, 324 (1993).
- [39] L. Roters, A. Hucht, S. Lübeck, U. Nowak, and K. D. Usadel, Depinning transition and thermal fluctuations in the random-field Ising model, *Phys. Rev. E* **60**, 5202 (1999).
- [40] A. Rosso, A. K. Hartmann, and W. Krauth, Depinning of elastic manifolds, *Phys. Rev. E* **67**, 021602 (2003).
- [41] A. Rosso, P. Le Doussal, and K. J. Wiese, Numerical calculation of the functional renormalization group fixed-point functions at the depinning transition, *Phys. Rev. B* **75**, 220201(R) (2007).
- [42] E. E. Ferrero, S. Bustingorry, and A. B. Kolton, Non-steady relaxation and critical exponents at the depinning transition, *Phys. Rev. E* **87**, 032122 (2013).
- [43] S. Ramanathan and D. S. Fisher, Onset of propagation of planar cracks in heterogeneous media, *Phys. Rev. B* **58**, 6026 (1998).
- [44] S. Zapperi, P. Cizeau, G. Durin, and H. E. Stanley, Dynamics of a ferromagnetic domain wall: Avalanches, depinning transition, and the Barkhausen effect, *Phys. Rev. B* **58**, 6353 (1998).
- [45] A. Rosso and W. Krauth, Roughness at the depinning threshold for a long-range elastic string, *Phys. Rev. E* **65**, 025101(R) (2002).
- [46] O. Duemmer and W. Krauth, Depinning exponents of the driven long-range elastic string, *J. Stat. Mech.* (2007) P01019.
- [47] L. Laurson, X. Illa, S. Santucci, K. Tore Tallakstad, K. J. Måløy, and M. J. Alava, Evolution of the average avalanche shape with the universality class, *Nat. Commun.* **4**, 3927 (2013).
- [48] H.-H. Boltz and J. Kierfeld, Depinning of stiff directed lines in random media, *Phys. Rev. E* **90**, 012101 (2014).
- [49] L.-H. Tang, M. Kardar, and D. Dhar, Driven Depinning in Anisotropic Media, *Phys. Rev. Lett.* **74**, 920 (1995).
- [50] A.A. Fedorenko, P. Le Doussal, and K.J. Wiese, Statics and dynamics of elastic manifolds in media with long-range correlated disorder, *Phys. Rev. E* **74**, 061109 (2006).
- [51] S. Bustingorry, A. B. Kolton, and T. Giamarchi, Random-manifold to random-periodic depinning of an elastic interface, *Phys. Rev. B* **82**, 094202 (2010).
- [52] L. A. Nunes Amaral, A. L. Barabási, and H. E. Stanley, Universality Classes for Interface Growth with Quenched Disorder, *Phys. Rev. Lett.* **73**, 62 (1994).
- [53] A. Rosso and W. Krauth, Origin of the Roughness Exponent in Elastic Strings at the Depinning Threshold, *Phys. Rev. Lett.* **87**, 187002 (2001).
- [54] T. Goodman and S. Teitel, Roughness of a tilted anharmonic string at depinning, *Phys. Rev. E* **69**, 062105 (2004).

- [55] P. Le Doussal and K. J. Wiese, Functional renormalization group for anisotropic depinning and relation to branching processes, *Phys. Rev. E* **67**, 016121 (2003).
- [56] Y. J. Chen, S. Zapperi, and J. P. Sethna, Crossover behavior in interface depinning, *Phys. Rev. E* **92**, 022146 (2015).
- [57] L. E. Aragón, A. B. Kolton, P. L. Doussal, K. J. Wiese, and E. A. Jagla, Avalanches in tip-driven interfaces in random media, *Europhys. Lett.* **113**, 10002 (2016).
- [58] A. Glatz, T. Nattermann, and V. Pokrovsky, Domain wall Depinning in Random Media by AC Fields, *Phys. Rev. Lett.* **90**, 047201 (2003).
- [59] C. ter Burg, F. Bohn, F. Durin, R. Sommer, and K. Wiese, Force correlations in disordered magnets, [arXiv:2109.01197](https://arxiv.org/abs/2109.01197).
- [60] L. Albornoz, E. Ferrero, A. Kolton, V. Jeudy, S. Bustingorry, and J. Curiale, Universal critical exponents of the magnetic domain wall depinning transition, *Phys. Rev. B* **104**, L060404 (2021).
- [61] D. Ertas and M. Kardar, Anisotropic scaling in threshold critical dynamics of driven directed lines, *Phys. Rev. B* **53**, 3520 (1996).
- [62] A. E. Koshelev and A. B. Kolton, Theory and simulations on strong pinning of vortex lines by nanoparticles, *Phys. Rev. B* **84**, 104528 (2011).
- [63] L. Civale, Pushing the limits for the highest critical currents in superconductors, *Proc. Natl. Acad. Sci. USA* **116**, 10201 (2019).
- [64] A. A. Middleton, Asymptotic Uniqueness of the Sliding State for Charge-Density Waves, *Phys. Rev. Lett.* **68**, 670 (1992).
- [65] A. Dobrinevski, P. Le Doussal, and K. J. Wiese, Non-stationary dynamics of the Alessandro-Beatrice-Bertotti-Montorsi model, *Phys. Rev. E* **85**, 031105 (2012).
- [66] A. Dobrinevski, P. Le Doussal, and K. Wiese, Avalanche shape and exponents beyond mean-field theory, *Europhys. Lett.* **108**, 66002 (2014).
- [67] A. Rosso and W. Krauth, Monte Carlo dynamics of driven strings in disordered media, *Phys. Rev. B* **65**, 012202 (2001).
- [68] H. Leschhorn and L.-H. Tang, Comment on “Elastic String in a Random Potential”, *Phys. Rev. Lett.* **70**, 2973 (1993).
- [69] P. Grassberger, D. Dhar, and P. K. Mohanty, Oslo model, hyperuniformity, and the quenched Edwards-Wilkinson model, *Phys. Rev. E* **94**, 042314 (2016).
- [70] A. Shapira and K. Wiese (unpublished).
- [71] A. E. Koshelev and V. M. Vinokur, Dynamic Melting of the Vortex Lattice, *Phys. Rev. Lett.* **73**, 3580 (1994).
- [72] A. B. Kolton, R. Exartier, L. F. Cugliandolo, D. Domínguez, and N. Grønbech-Jensen, Effective Temperature in Driven Vortex Lattices with Random Pinning, *Phys. Rev. Lett.* **89**, 227001 (2002).
- [73] A. B. Kolton, Pinning induced fluctuations on driven vortices, *Phys. C (Amsterdam)* **437-438**, 153 (2006).
- [74] G. Blatter, M. V. Feigel'man, V. B. Geshkenbein, A. I. Larkin, and V. M. Vinokur, Vortices in high-temperature superconductors, *Rev. Mod. Phys.* **66**, 1125 (1994).
- [75] M. Tinkham, *Introduction to Superconductivity*, 2nd ed. (Dover, New York, 2004).
- [76] P. Le Doussal and K. Wiese, How to measure Functional RG fixed-point functions for dynamics and at depinning, *Europhys. Lett.* **77**, 66001 (2007).
- [77] P. L. Doussal, K. Wiese, S. Moulinet, and E. Rolley, Height fluctuations of a contact line: A direct measurement of the renormalized disorder correlator, *Europhys. Lett.* **87**, 56001 (2009).
- [78] K. J. Wiese, M. Bercy, L. Melkonyan, and T. Bizebard, Universal force correlations in an RNA-DNA unzipping experiment, *Phys. Rev. Research* **2**, 043385 (2020).
- [79] C. ter Burg and K. J. Wiese, Mean-field theories for depinning and their experimental signatures, *Phys. Rev. E* **103**, 052114 (2021).
- [80] P. LeDoussal and K. J. Wiese, Driven particle in a random landscape: Disorder correlator, avalanche distribution and extreme value statistics of records, *Phys. Rev. E* **79**, 051105 (2009).
- [81] P. LeDoussal, K. J. Wiese, and P. Chauve, Functional renormalization group and the field theory of disordered elastic systems, *Phys. Rev. E* **69**, 026112 (2004).
- [82] L. Ponson (private communication, 2021).
- [83] M. Grassi, A. B. Kolton, V. Jeudy, A. Mougín, S. Bustingorry, and J. Curiale, Intermittent collective dynamics of domain walls in the creep regime, *Phys. Rev. B* **98**, 224201 (2018).
- [84] A. Rosso, P. Le Doussal, and K. J. Wiese, Avalanche-size distribution at the depinning transition: A numerical test of the theory, *Phys. Rev. B* **80**, 144204 (2009).
- [85] P. Le Doussal, A. A. Middleton, and K. J. Wiese, Statistics of static avalanches in a random pinning landscape, *Phys. Rev. E* **79**, 050101(R) (2009).
- [86] C. J. Bolech and A. Rosso, Universal Statistics of the Critical Depinning Force of Elastic Systems in Random Media, *Phys. Rev. Lett.* **93**, 125701 (2004).
- [87] A. A. Fedorenko, P. Le Doussal, and K. J. Wiese, Universal distribution of threshold forces at the depinning transition, *Phys. Rev. E* **74**, 041110 (2006).
- [88] A. B. Kolton, A. Rosso, T. Giamarchi, and W. Krauth, Creep dynamics of elastic manifolds via exact transition pathways, *Phys. Rev. B* **79**, 184207 (2009).
- [89] L. F. Cugliandolo, The effective temperature, *J. Phys. A: Math. Theor.* **44**, 483001 (2011).
- [90] P. Le Doussal, A. Petković, and K. J. Wiese, Distribution of velocities and acceleration for a particle in Brownian correlated disorder: Inertial case, *Phys. Rev. E* **85**, 061116 (2012).
- [91] J. Sparfel and K. Wiese (unpublished).
- [92] S. Ramanathan, D. Ertas, and D. S. Fisher, Quasistatic Crack Propagation in Heterogeneous Media, *Phys. Rev. Lett.* **79**, 873 (1997).
- [93] D. Dalmas, A. Lelarge, and D. Vandembroucq, Crack Propagation through Phase-Separated Glasses: Effect of the Characteristic Size of Disorder, *Phys. Rev. Lett.* **101**, 255501 (2008).